J Biosci Vol. 43, No. 3, July 2018, pp. 519–540
DOI: 10.1007/s12038-018-9769-y

Single-molecule fluorescence imaging: Generating insights into molecular interactions in virology

SUNAINA BANERJEE[1,†], SATYAGHOSH MAURYA[2,†] and RAHUL ROY[1,2,3]*

[1]*Molecular Biophysics Unit, Indian Institute of Science, Bengaluru, India*

[2]*Department of Chemical Engineering, Indian Institute of Science, Bengaluru, India*

[3]*Centre for Biosystems Science and Engineering, Indian Institute of Science, Bengaluru, India*

**Corresponding author (Email, rahulroy@iisc.ac.in)*

[†]*These authors contributed equally to this work.*

Published online: 25 June 2018

Single-molecule fluorescence methods remain a challenging yet information-rich set of techniques that allow one to probe the dynamics, stoichiometry and conformation of biomolecules one molecule at a time. Viruses are small (nanometers) in size, can achieve cellular infections with a small number of virions and their lifecycle is inherently heterogeneous with a large number of structural and functional intermediates. Single-molecule measurements that reveal the complete distribution of properties rather than the average can hence reveal new insights into virus infections and biology that are inaccessible otherwise. This article highlights some of the methods and recent applications of single-molecule fluorescence in the field of virology. Here, we have focused on new findings in virus–cell interaction, virus cell entry and transport, viral membrane fusion, genome release, replication, translation, assembly, genome packaging, egress and interaction with host immune proteins that underline the advantage of single-molecule approach to the question at hand. Finally, we discuss the challenges, outlook and potential areas for improvement and future use of single-molecule fluorescence that could further aid our understanding of viruses.

Keywords. Fluorescence correlation spectroscopy; Förster resonance energy transfer; single molecule fluorescence; single molecule virology; single particle tracking; super-resolution microscopy

1. Introduction

Mammalian viruses form a large class of nanometer-scale, small proteome organisms that use the target host cells to replicate and propagate. In spite of progress made with antivirals and vaccines, viral pathogens still represent a large public health burden in many developing countries with continued emergence of new strains (Woolhouse and Gowtage-Sequeria 2005; Jones *et al.* 2008; Howard and Fletcher 2012). Drug and vaccine design against viruses are driven by conventional 'screening' as well as rational design-based approaches (Quan *et al.* 1998; Finco and Rappuoli 2014). In both the cases, mechanistic understanding of molecular function, dynamics and interactions can provide profound and useful insight to inhibit key viral processes. In this review, we make a case for application of single-molecule fluorescence as a complementary tool to structural biology, functional activity assays and ensemble spectroscopic techniques. We review the current progress in the field of single-molecule virology, highlighting the studies that generated mechanistic understanding of viral protein, genome activity and function, viral lifecycle processes and their interactions with the host components.

Virus lifecycle involves a complex interplay of virus and host cell interactions that determines the infection outcome (figure 1a). The virus infection cycle starts by binding to receptors and/or membrane on the host cell surface. Most viruses enter the cell through endocytosis and, despite variations in structure and size, display commonalities in trafficking (Pelkmans and Helenius 2003; Marsh and Helenius 2006). After internalization, the viral genome release from endosomes into the cytoplasm occurs either by viral membrane fusion to the endosomal membrane (most enveloped viruses) or by disruption (or fusion) of the cellular membrane (most non-enveloped viruses). This is followed by key viral lifecycle processes, that is, replication of the viral genome to produce its progeny and translation of the additional viral proteins that are required for new rounds of replication, packaging of the new virus and other essential processes. The order and sites for these processes varies depending on the virus with viral proteins continuously interacting with cellular organelles and host proteins during their lifecycle. Finally, assembly and packaging of the new viral genomes into virus particles is followed by budding,

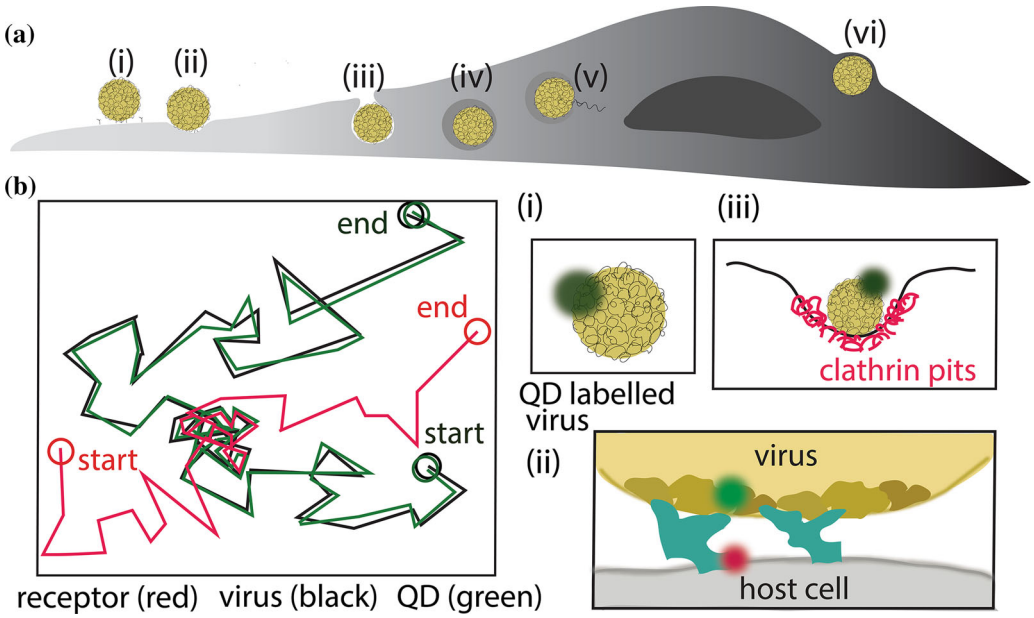

Figure 1. Single-particle fluorescence-based tracking can monitor major steps in virus trafficking to and inside a host cell. (**a**) Schematic overview of the events of viral entry into a mammalian cell that can be explored with single virus or protein imaging experiments (not to scale) (i) Diffusion of the virus on a mammalian cell surface can be monitored in real time by fluorescently labelling the viral outer coat (e.g. with Quantum dots, QD). (ii) Attachment of the virus to the mammalian cell surface mediated by host–receptor interactions can be studied by high-resolution fluorescence co-localization. (iii) Endocytosis of the virus in clathrin-coated pits can be similarly tracked by co-localization. (iv) Endosomal maturation–associated virus fates can be measured using co-localization with endosomal markers. (v) Membrane fusion tracked by dequenching of virus membrane labels followed by release of the viral genome can be monitored with markers that bind the genome specifically. (vi) Budding and egress can be followed with labelled coat proteins along with host factors. (**b**) Representative particle tracks where the virus centroid (interferometric signal, black) and the peripherally attached tag (quantum dot fluorescence, green) signals are observed as it diffuses along the cell surface. The scattering from the virus could be used along with QD to monitor the orientation in which the virus binds to the cell surface. Simultaneous host protein tracking (red) and co-localization of all tracks can be used to infer specific interactions and kinetics of the processes.

exocytosis or cell lysis. The new virions thus released go on to infect new cells.

One might ask, what is the need to study viruses at the single-molecule level (i.e. to characterize each molecule or virus individually)? Technically, single-molecule measurements represent the highest level of sensitivity and hence do not require perturbations like over-expression or excessive labelling of molecules to probe systems. More importantly, they do not require synchronization of biological reactions and processes, and can detect transient, yet significant, intermediates. In fact, the intrinsic stochastic nature of reactions is best evident at the single-molecule level. This also allows one to dissect reaction pathways and kinetics and identify on- and off-pathway mechanisms (Weiss 1999; Walter *et al.* 2008). Additionally, kinetics and thermodynamics can be measured simultaneously since the molecules continue to undergo forward and backward reactions at the rates defined by the thermodynamic barriers even under equilibrium conditions.

Single-molecule methods become more relevant when the biological process is inherently initiated and dependent on the activity and function of a small number of molecules as in the case of virus infections. Viruses comprise small number of structural proteins that form their coat and a few copies of enzymes and usually consist of a single copy of nucleic acid as its genome. Viral infections also start from small number of infectious units, and hence stochastic effects likely control the infection kinetics and outcome. Additionally, virus infections are intrinsically heterogeneous processes (i.e. variable over several scales both spatially and in composition) with their properties and distributions changing with time. Combined with similarly heterogeneous host cell interactions and changes induced by the viral infection, inferences from ensemble averaged data is extremely challenging (Snijder *et al.* 2009; Heldt *et al.* 2015; Ramanan *et al.* 2016). Several prior reviews have illustrated the differences between single-molecule and ensemble experiments elegantly and highlighted various single-molecule-based case studies in biology and we refer the reader to those for brevity (Weiss 1999; Moerner and Fromm 2003; Joo *et al.* 2008; Tinoco and Gonzalez 2011). In line with the focus of the special issue, we have reviewed the single-molecule- and single-virion-based fluorescence methods commonly employed in virology and underscored the new

insights generated that were otherwise difficult to establish with conventional methods. We focus on viral entry, virus membrane fusion, viral protein interactions with nucleic acids relevant to replication and translation and finally virus assembly and packaging highlighting the common single-molecule fluorescence strategies used to study such processes and the understanding generated in some select cases.

2. Single-virus particle dynamics

Visualization of single viruses as they undertake infection of the cell has been a long-coveted goal that has become possible with the advent of multiple ways to label viruses without loss of infectivity and advent of highly sensitive and fast detectors (Seisenberger *et al.* 2001; Brandenburg and Zhuang 2007; Rust *et al.* 2011; Sivaraman *et al.* 2011). Usually virus imaging employs a fluorescently labelled virus particle that is monitored over different phases of its life-cycle in the live cell. To ensure efficient labelling of the virus without hampering its infectivity, several approaches have been demonstrated successfully (Lakadamyali *et al.* 2003; Finke *et al.* 2004; van der Schaar *et al.* 2008; Rust *et al.* 2011; Lelek *et al.* 2012; Sun *et al.* 2013; Wang *et al.* 2013). When isolation of the viruses is possible in high concentrations and purity, one can resort to organic fluorescent dyes to label the viral membrane (lipophilic dyes) or viral coat proteins (covalent conjugation chemistries that target lysine or cysteine residues). Quantum dots (Q-dot) or gold (Au) nanoparticles are also used occasionally to label the outer coat or envelope protein if the size of the probe does not hamper virus infection. Additionally, genomic (nucleic acid) probes such as those used in fluorescence *in situ* hybridization (FISH) are employed to directly follow the sites of genome processing (Chou *et al.* 2013). In some cases, infectious viruses with fluorescent protein fusions to viral proteins have been possible, enabling generation of genetically tagged viral particles (Finke *et al.* 2004; Kobiler *et al.* 2011; Avilov *et al.* 2012; Schoggins *et al.* 2012; Granstedt *et al.* 2013; Hoornweg *et al.* 2016; Maier *et al.* 2016; Sood *et al.* 2017; Vanover *et al.* 2017). The host cell is further tagged either on the membrane or on the corresponding virus receptors to enable simultaneous imaging of the interacting partners.

Epi- (including highly inclined thin illumination (HILO) mode), confocal- and total internal reflection-based microscopy are the most popular methods for single-particle detection and tracking (Axelrod 1981; Sako *et al.* 2000; Stephens and Allan 2003; Tokunaga *et al.* 2008; Rust *et al.* 2011). Rapid movement of the virus particle in the vicinity of the cell is captured in movies using fluorescence microscopy. Diffraction-limited images of the virus particles are identified by intensity thresholding, followed by fitting the image to a mathematical function (usually a 2D Gaussian) to estimate the centroid of the particle. Centroids of the virus particle from subsequent frames of the movie are then connected to generate a particle trajectory (figure 1b). Next, the particle trajectories are analysed for the type of motion (random diffusion, restricted diffusion, or directed motion), speed of movement and time-dependent intensity changes revealing the underlying transport processes and interactions. Co-localization of the trajectory with cellular components like receptors can further reveal the time scale and nature of contacts (figure 1b). Furthermore, similar fluorescence trajectories of the virus can be co-localized with other trajectories including those from other imaging modalities (figure 1b). Using such an approach with scattering interferometry that reports on virus particle centroids and comparing it to centroid of Q-dots located on virus periphery, the position and orientation of the virus could be measured with sub-nanometer spatial and less than 10 ms temporal resolution (Kukura *et al.* 2009).

For the non-enveloped viruses, labelling of the capsid proteins has allowed tracking of the viruses, and genome release could be monitored post-infection. One of the first reports of single-virus tracking of Adeno-associated virus (AAV) in HeLa cells displayed heterogeneous diffusive behaviour on cell membrane and post-cell entry ($D \sim 0.4$-$7\ \mu m^2/s$) (Seisenberger *et al.* 2001). After rapid endocytosis, AAV motion was characterized by anomalous diffusion in the endosomes or directed motion possibly under the influence of motor proteins. Such heterogeneous movement, a common feature observed in virus tracking experiments, is masked in other 'coarser' approaches and highlights the underlying need of probing particle movements individually. More recent work has described how viruses use cortical actin cytoskeleton and cell surface attachment factors to 'surf', search and activate binding to specific receptors and cell entry sites (Lehmann *et al.* 2005; Coyne and Bergelson 2006). Combining multi-colour imaging with virus tracking has helped resolve the underlying principles for cellular entry and transport. When the simian virus 40 (SV40) was co-visualized with the caveolae, a two-step pathway for delivery of the virus to the smooth endoplasmic reticulum (ER) was discovered (Pelkmans *et al.* 2001). After entrapment of the virus in the small caveolin vesicles, these vesicles would merge with larger caveolin-rich organelles (caveolosome). Viruses would then be sorted in caveolin-free vesicles and undertake microtubule-guided movement to the ER for genome delivery. On the other hand, Polio virus (PV), tracked in a similar fashion, entered the cell via the endocytic pathway that was independent of clathrin or caveolin and did not involve the microtubules (Brandenburg *et al.* 2007). On the other hand, depletion of ATP, inhibition of tyrosine kinases and disruption of actin microfilaments led to a complete loss of infection events. By simultaneously labelling the viral RNA, they further showed that the PV genome was released from the encapsulating vesicles close

to the cell membrane surface after inducing conformational changes in the viral capsid and formation of the viral pore complex. Therefore, non-enveloped viruses employ a multitude of clathrin-independent endocytic pathways instead of disrupting the plasma membrane directly to achieve productive entry into the host cell.

Enveloped RNA viruses that require an obligatory membrane fusion step have been studied using viral membrane labelling with lipophilic dyes and co-localizing them with endocytic pathway markers. The influenza virus displayed distinct and highly heterogeneous entry and transport pathways in the cell (Lakadamyali *et al.* 2003; Rust *et al.* 2004; Lakadamyali *et al.* 2006). The motion of the influenza particles on the cell surface was found to be actin dependent in the initial stages that switched to dynein-dependent movement on microtubules towards the perinuclear region post endocytic entry (Lakadamyali *et al.* 2003). About two-thirds of the virus particles underwent Clathrin-dependent endocytosis by *de novo* formation of clathrin-coated pits and the rest entered the cell using clathrin- and caveolin-independent pathways (Rust *et al.* 2004). The virus was also selectively sorted into a highly mobile pool of early endosomes (Lakadamyali *et al.* 2006). Eventual fusion of the viruses measured by dequenching of the viral membrane dye occurred after this microtubule-dependent transport and was dependent on this transport. Co-localization with Rab5 and Rab7 endosome markers showed how the fusion typically happened during the endosomal maturation process. In case of the dengue (DENV) virus, another enveloped virus, binding to cells was extremely poor, which could explain its poor infectious unit-to-viral particle ratio (van der Schaar *et al.* 2007). Dengue virus gains cell entry exclusively via clathrin-mediated endocytosis (van der Schaar *et al.* 2008). However, unlike influenza, DENV particles diffusively searched the cell membrane till they were arrested on clathrin-coated pits. Once endocytosed, only one-sixth of the DENV viruses displayed complete fusion that occurred in Rab5/Rab7-rich late endosomes. Therefore, such single-virus tracking studies in combination with inhibitors and antibodies can reveal cell receptor-mediated virus interactions and viral cell entry pathways which are potent targets for intervention.

3. Protein–membrane interactions

Another crucial interaction that modulates viral infection is the virus interaction with cellular membranes. After the initial search for receptor and binding (as discussed earlier), enveloped viruses must undergo membrane fusion either with the cytoplasmic membrane or with the endosome membrane (after endocytosis) to deliver their genome into the cytoplasm for viral translation and replication. The viral membrane fusion process is a heterogeneous multi-step process with large kinetic barriers (Chernomordik and Kozlov 2003). Despite differences in the structure and size, all enveloped viruses employ dedicated envelope proteins that reside on the viral membrane in a broadly similar mechanism to achieve membrane fusion (Harrison 2008, 2015; White and Whittaker 2016). Envelope proteins, often triggered by a ligand binding (such as protons in the endosome or receptors/co-receptors on the cell surface), undergo large conformational changes and expose lipophilic 'fusion' regions. Insertion of these hydrophobic segments into the cellular membrane links the two membranes. Further structural changes in the envelope protein bring the two membranes closer together and thereby catalyse the fusion process. *In vitro* fluorescence assays that probe membrane fusion have been used with fluorescently labelled virus particles that bind and fuse to a cell membrane and/or artificial bilayer when triggered by envelope protein activation (Otterstrom and van Oijen 2013). Using TIRF microscopy to limit background, various stages of the virus membrane interaction can be studied where the viral membrane as well as the content (for example, the genome) is labelled with two distinct fluorophores. Approach and binding of the virus to the host cell (or membrane-bound receptors on supported bilayer) is observed as an abrupt appearance of a fluorescent signal (in a diffraction limited spot) on the membrane (figure 2a). This abrupt change in fluorescence intensity is largely due to the limited lateral mobility of the virus on the lipid membrane compared with 3D diffusion in the solution as well as selective illumination of the membrane using evanescent field from total internal reflection. Similarly, unbinding events as (abrupt) disappearance of the spots can be used to study the binding affinity of the membranes/receptors to the virus. Next, fusion of the viral membrane to the target membrane can be followed with a change in the intensity of the lipophilic dye. Several lipid dyes can be incorporated on the virus membrane at high self-quenching concentrations ($\sim$ 2–5 mole percent of total viral lipids) without compromising virus infectivity. Mixing and subsequent diffusion of these quenched lipid dyes upon viral membrane fusion with the target membrane causes a transient enhancement of the fluorescence signal, followed by a gradual drop at the site of fusion (figure 2b). If the acquisition is fast compared to the fusion kinetics, fusion intermediates like the hemi-fusion state (fusion of outer leaflets of the bilayer membrane) can also be captured as intermediate steps in the fluorescence changes observed. Finally, the release of the viral content can be measured by drop in content (water-soluble) dye fluorescence ('turn-off' assay) due to diffusion after release or fluorescence enhancement due to interaction of the contents with the external component (figure 2c). The water-soluble dyes are usually incorporated by long incubation of the dye with the virus, followed by gel filtration or dialysis. Several recent advances like the ability to generate supported bilayer platforms from

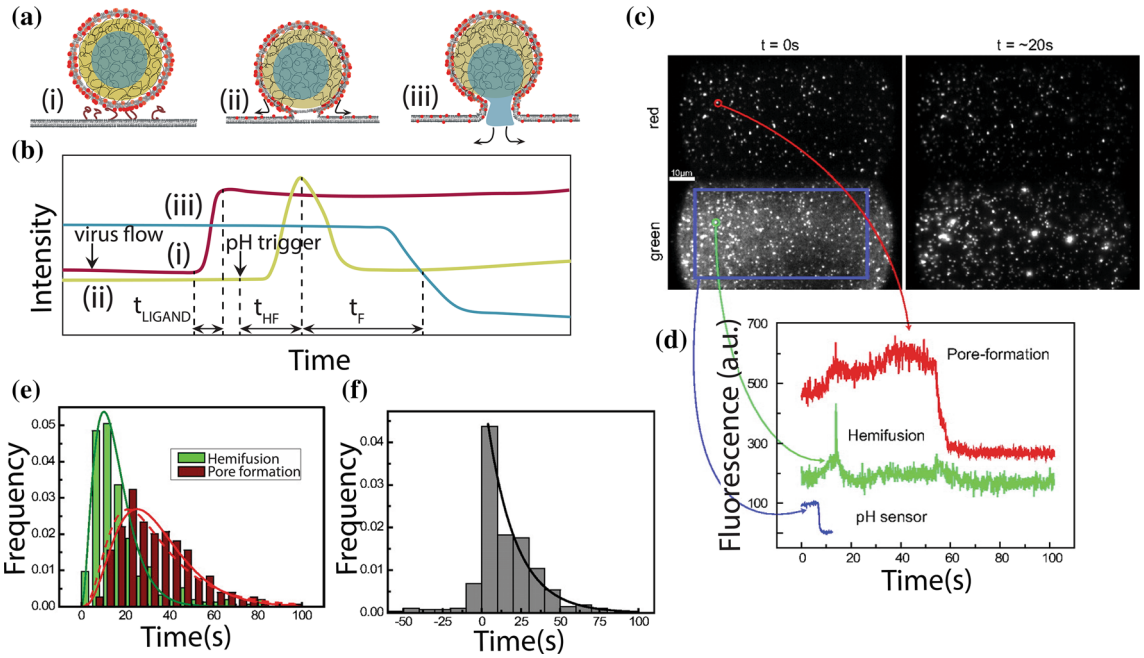

Figure 2. Single-viral membrane fusion and genome release assays (Floyd *et al.* 2008). (**a**) Schematic of a fluorescent virus particle binding and fusing onto an artificial lipid membrane. The viral membrane is labelled with a quenched dye (red) and fusion to the artificial lipid membrane will re-distribute the dye, resulting in dequenching of the fluorescence signal. The nucleic acid (genome, blue) is labelled with spectrally distinct fluorophores and its release and diffusion can be monitored separately. (**b**) Time trajectory of a single virus fusion event is shown schematically. (i) When the virus binds to the cell surface receptors, appearance of a fluorescence spot (red) could be obtained due to restricted diffusion on the surface. This signal could be from a fluorescent tag on the Env or a lipophilic dye in the membrane of the virus or signal from a fluorescently tagged genome. If the quenched lipophilic dye is present on the viral membrane, fusion of the membranes can be tracked in further detail. (ii) As the two membranes fuse together, rapid dequenching due to mixing of the membranes will increase fluorescence (yellow) with time signifying the hemi-fusion step. Full fusion will lead to redistribution of the dye within the target bilayer, resulting in decline in this intensity level to values prior to fusion. (iii) Dye on the nucleic acid is released in bulk along with the capsid–nucleic acid complex and a drop in this intensity at the fusion site reports on genome release (blue). t_{Ligand} represents time interval when the virus diffuses near the membrane till it is captured by the host receptor. t_{HF} and t_F represent the time intervals for hemi-fusion post trigger and full-fusion from hemi-fusion state. (**c**) Fluorescence images of virus fusion assay. In a three-dye experiment, a pH sensor, the labelled viral genomic content and labelled membrane are simultaneously observed with time. (**d**) Representative time traces from the single viral fusion assay, viz. the pH drop (blue), hemi-fusion (green) and fusion (red) states can be acquired and estimated. (**e**) Decoupling the fusion kinetic pathway is possible by fitting lag times between the pH trigger and hemi-fusion (green, t_{HF}) and pore formation (red, $t_{HF}+t_F$) to gamma functions. (**f**) The distribution of time delays obtained between hemi-fusion and pore formation ($t_{F)}$ are best fit to an exponential decay, indicating a single rate-limiting step in achieving full fusion post hemi-fusion. Figure 2c–f is adapted with permission from Floyd *et al.* by The National Academy of Sciences of the USA.

cellular membranes (containing all relevant receptors and local photo-uncaging based changes in the pH and other molecules) are enabling increasing levels of sophistication in such measurements (Costello *et al.* 2012, 2013).

In an early influenza virus membrane fusion study that employed several of the strategies outlined earlier, a pH-dependent membrane fusion assay was used to monitor the hemi-fusion and fusion kinetics by van Oijen and Harrison groups (Floyd *et al.* 2008). In addition to the virus membrane and content labelling, the lipid bilayer was labelled with a pH sensor dye and supported on dextran polymer cushion to monitor pH change and promote efficient virus fusion, respectively. Gamma distribution function fitting of the hemi-fusion time distributions (time taken to observe dequenching of lipophilic dye from the point of pH change) revealed at least three intermediate steps before the formation of hemi-fusion stalk, suggesting the requirement for three hemagglutinin (HA) trimers for successful hemi-fusion (figure 2d–2f). Extending the same approach to measure the fusion kinetics of mutant HA proteins, Ivanovic *et al.* determined that the release of the fusion peptide from its pocket near the threefold axis regulated the formation rate of a long-lived extended intermediate (Ivanovic *et al.* 2013). They also compared dwell-time distributions of various fusion intermediates observed in the assay to simulations of molecular events underlying the fusion and described how

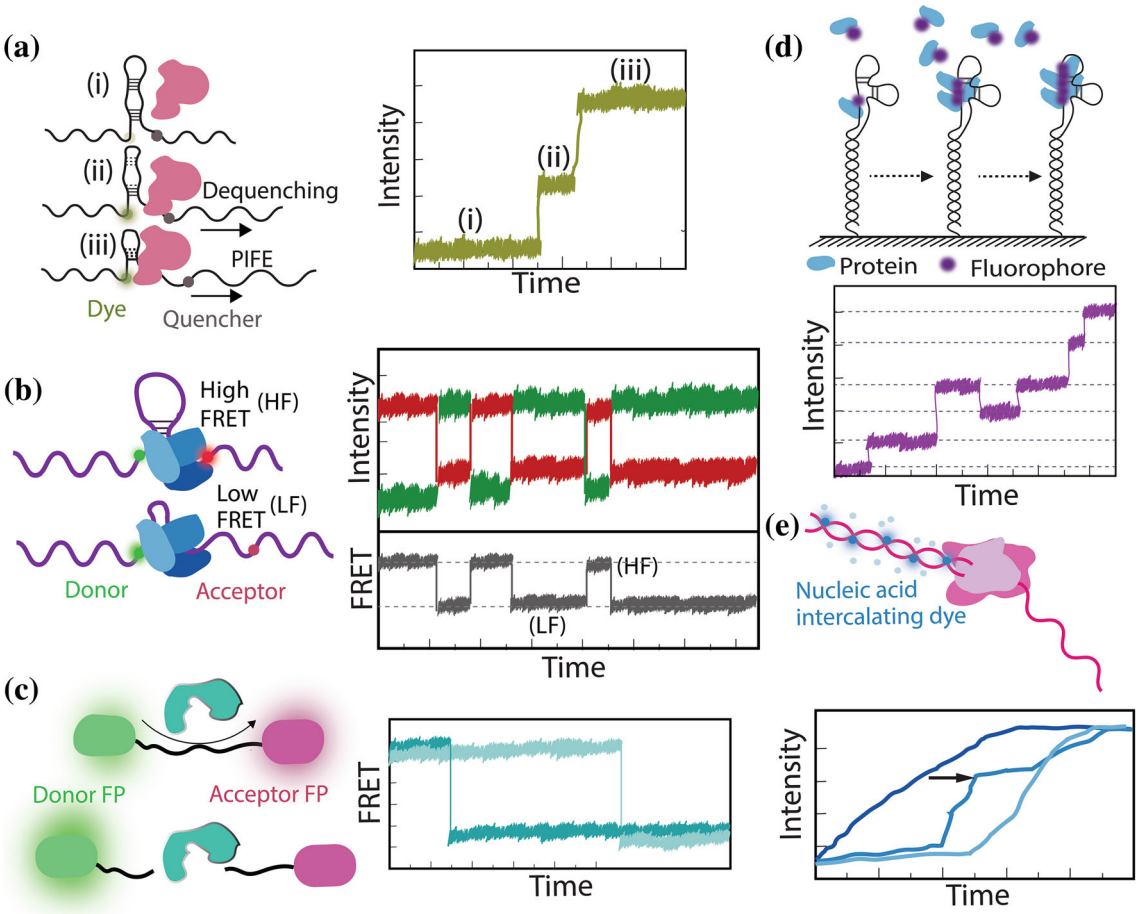

Figure 3. Nucleic acid interactions with viral proteins. (**a**) Quenching assay in combination with smPIFE to monitor nucleic acid remodelling by a protein. Increase in inter-dye distance leads to dequenching of dye (placed originally in the vicinity of a quencher molecule) as the polymerase disrupts base-pairing locally (i → ii) and further enhancement of intensity in signal is observed due to fluorescent enhancement induced by the protein (ii → iii). (**b**) Real-time FRET-based monitoring of a helicase unwinding of a nucleic acid stem-loop structure. A reversible FRET signal decrease is observed when the inter-dye distance increases due to rapid disruption of the stem-loop structure. (**c**) Protease activity can be similarly monitored on a peptide substrate labelled with a fluorescent protein (FP) FRET pair. The abrupt decrease in FRET efficiency is used to determine the kinetics of protease activity. (**d**) Labelled protein spontaneously oligomerizing upon binding to nucleic acid can be estimated with tracking the step-wise changes in the intensity of the diffraction-limited spots that is indicative of the number and binding/dissociation of protomers. (**e**) Scheme for the real-time measurement of polymerization by an RNA polymerase. Formation of the dsRNA by an RNA polymerase can be measured in real time via nucleic acid binding–induced emission (enhancement of a dsRNA selective dye). The three model trajectories (blue traces) represent the activity of individual polymerases on three RNA molecules with slopes corresponding to rate of polymerization. An intermediate (arrow) no-activity regime in a trace might represent a polymerase fall-off or a stalled complex.

the hemi-fusion proceeded rapidly upon the availability of three or four 'adjacent' HA trimers in the membrane-inserted state. Single-virus particle studies with West Nile virus (WNV, a representative of the flavivirus family) have also shown that the envelope protein, which is present as a dimer in the mature virus membrane, undergoes sequential steps of dimer dissociation, conformational change to form the extended state that exposes the fusion loop, followed by a much slower trimer formation that regulated the fusion process (Chao *et al.* 2014). The last step was controlled by the availability of the adjacent extended monomers akin to the case of influenza, but the critical number required for hemi-fusion was determined to be two molecules for flaviviruses, such as WNV and Kunjin virus. In a slightly different configuration, Wessels *et al.* first reported the pH-induced change in the Sindbis virus fusion protein, and observed rapid binding and fusion kinetics to target lipid membranes (Wessels *et al.* 2007). Sindbis virus fusion was not only dependent on the membrane composition (cholesterol levels) but also the fusion kinetics slowed down at low

pH. On the other hand, Influenza virus fusion was unaffected under the same range of conditions. This suggests that the role of membrane lipid groups, solution conditions and the fusion protein play a role in regulating the fusion kinetics even at the refolding stage of the fusion protein activity. Floyd *et al.* also demonstrated that bilayer mixing preceded full pore formation by measuring the elapsed time between hemi-fusion and content release (figure 2e) (Floyd *et al.* 2008). The single exponential dwell-time distribution of the hemi-fusion state prior to fusion was consistent with a single rate-limiting step controlling the transition from membrane fusion to content release.

Unlike simple fusion triggers, like acidic pH discussed earlier, the HIV-1 envelope (Env) a protein that is organized as a mushroom-shaped trimer of heterodimers of gp120/gp41, requires receptor (CD4) binding that induces an initial conformational change and exposes a co-receptor–binding surface (Blumenthal *et al.* 2012). Upon further co-receptor (CXCR4 or CCR5) binding and activation of Env, full fusion is achieved. Single-molecule FRET studies demonstrated that native HIV-1 Env trimers can exist in a dynamic equilibrium of three distinct pre-fusion structures representing the ground-state conformation, one that was stabilized by CD4 with a co-receptor mimic and an uncharacterized structural state that was an obligatory intermediate during the activation of Env by CD4 (Munro *et al.* 2014). This enabled not only the direct validation of the two-step activation by CD4 and co-receptors of gp120 but also the characterization of modulation of these states by neutralizing antibodies and inhibitors. Several questions still remain regarding the catalytic mechanism of HIV-1 Env mediated fusion like the conformational dynamics and stoichiometry of extended gp41 trimers required for fusion that shall be addressed in the future with the development of new labelling strategies using non-canonical amino acids (Sakin *et al.* 2017).

Membrane composition and heterogeneity also can determine the protein-induced fusion kinetics. For example, cholesterol-rich 'raft' domains are known to be vital for insertion of fusion peptide of HIV gp41 and HIV cell entry (Yang *et al.* 2015, 2016). Using the HIV fusion peptide and pseudotyped HIV binding to artificial membranes, Yang *et al.* showed that phase-segregated lipid bilayers that displayed co-existing ordered (Lo) and disordered (Ld) phases were more amenable to fusion and the HIV particles interacted and fused preferentially at boundaries between co-existing Lo and Ld lipid phases (Yang *et al.* 2015). Single-particle tracking of the HIV fusion peptide also displayed interconversion between different diffusive states that further confirm association of different membrane phases and possible peptide structures that might regulate the fusion dynamics (Ott *et al.* 2013). The exact molecular role of cholesterol or the phase-segregated bilayers in HIV and other envelope virus cell entry still needs to be evaluated.

4. Protein–nucleic acid interactions

Viral nucleic acid-binding proteins like polymerases and helicases form an important class of druggable targets because of their enzymatic nature. There have been continued efforts to develop functional assays to measure their binding, activity and structure–function relationship in the context of their interaction with nucleic acids. A key feature of any successful biological life process is an ability to exclusively and rapidly recognize and bind to its cognate partner to achieve functional outcome. This especially holds true for nucleic acid proteins from the virus, which despite favourable thermodynamics, must outcompete the high copy number host components for successful infection, a recurrent theme discussed here.

There have been several single-molecule fluorescence approaches that have been successfully employed in a variety of molecular systems to probe protein interaction with nucleic acids (Joo *et al.* 2008; Koh *et al.* 2016). One simple implementation of single-molecule fluorescence that utilizes the change in photophysical properties of the dye is protein-induced fluorescence enhancement, PIFE (Luo *et al.* 2007; Hwang and Myong 2014). By measuring the increase in the fluorescence emission upon protein binding in the vicinity of the dye, one can report on binding kinetics, equilibrium or non-equilibrium interactions between protein and the corresponding nucleic acid–binding site (figure 3a). Importantly, in spite of employing a single fluorophore, the 1 to 4 nm distance sensitivity and linearity of the effect on dye–protein separation ensures that local protein dynamics can be probed with high precision (Hwang and Myong 2014). Similarly, dye quenching has been employed to report on nucleic acid structure where proximity of dyes can report on the status of the conformation in real time (figure 3a). Förster resonance energy transfer (FRET) remains a popular single-molecule fluorescence method because of its ratiometric nature and nanometer sensitivity (Roy *et al.* 2008). In FRET, a donor fluorophore, when in its excited electronic state, can transfer its excitation energy to a nearby acceptor chromophore in a non-radiative fashion through long-range dipole–dipole interactions and efficiency of this energy transfer is mostly linear over 2–8 nm for most popular dye pairs. Placement of the dye pair (or any combination of donor and acceptor) on different parts of the potential nucleoprotein complex, and dynamic changes in the conformation of the molecular system can be measured (figure 3b). Another potential application of smFRET relevant to viral protease activity is monitoring the real-time cleavage activity of target proteins or peptides carrying a dye pair at their two ends (figure 3c). Because of the high signal-to-noise ratio achievable using current microscopy techniques like TIRF-microscopy (TIRFM) and use of photo-stabilizing agents, one can quantify binding of proteins to nucleic acid scaffolds directly (if the binding affinity is high and photo-

physics of the dye is unaltered upon binding) as step-wise changes in intensity at the binding site (figure 3d). Finally, more functional assays like polymerization of the nucleic acids by the viral proteins can be captured at the single-molecule level by using dyes specific to a double-stranded form of the product (figure 3e). These single-molecule fluorescence methods still primarily remain *in vitro* in nature, but several of them (e.g. smFRET) can be adapted for measurements inside live cells.

4.1 *Binding and oligomerization of viral proteins on nucleic acid*

Specific binding and oligomerization of the HIV-1 Rev protein on the highly conserved rev response element (RRE) of viral mRNA is critical to the activation of nuclear export of unspliced and partially spliced viral RNA (Daly *et al.* 1993; Mann *et al.* 1994). To probe the kinetic pathway and assembly intermediates of Rev oligomerization on RRE RNA, single-molecule fluorescence intensity measurements of labelled Rev proteins as they bind to the immobilized (truncated) RRE RNA was measured (Pond *et al.* 2009). Intensity jumps in the fluorescence time trajectories for single RNA corresponded to step sizes of a single Rev monomer, hence supporting the sequential binding model. This indicated that binding of a single Rev unit allows further assembly of additional monomers in contrast to a pre-formed assembly model in which pre-assembled Rev oligomers bind to the RRE. The high-affinity Rev-binding site in stem-loop IIB of the RRE displayed a maximum of four binding states and its deletion abolished the nucleation of Rev completely on the RRE. In a subsequent study, dwell time distributions of Rev oligomerization on the full-length RRE revealed two kinetic phases for the initial binding step, while dissociation had a single rate-limiting step (Robertson-Anderson *et al.* 2011). In the presence of human DEAD-box protein 1 (DDX1) helicase, a cellular host cofactor of the HIV-1 Rev, the second kinetic phase attributed to non-productive Rev nucleation events, was removed and it resulted in generation of higher-order Rev–RRE complexes (up to 8 Rev proteins per RRE). In a recent study, they further demonstrated that the DDX1 stimulation of Rev oligomerization was achieved by specific enhancement of the Rev nucleation step on the RRE (Lamichhane *et al.* 2017). In the light of smFRET experiments that demonstrated that DDX1 and Rev co-occupy the same RRE RNA with low probability, the proposed role of DDX1 is to remodel the RRE RNA conformation to prime it for Rev monomer binding.

The human immunodeficiency virus type 1 (HIV-1) reverse transcriptase (RT) plays an indispensable role in converting the ss-RNA viral genome to dsDNA required for insertion into the host genome. The physiologically characterized HIV-1 RT consists of two polypeptide chains, the 66 kDa (p66) which contains a polymerase and RNaseH domain and 51 kDa (p51) formed from the proteolytic cleavage of the p66 subunit during viral maturation, lacking the RNaseH domain (Starnes *et al.* 1988; Kohlstaedt *et al.* 1992). Additionally, the homodimers, p66-66 and p55-55 have been purified and studied, however little was understood about nucleic acid recognition and binding of the homodimers versus the functional heterodimer (Le Grice and Grüninger-Leitch 1990; Maier *et al.* 1999). Marko *et al*. used smPIFE to characterize binding of the heterodimeric and homodimeric HIV-1 reverse transcriptase (RT) with its Cy3-labelled primer-template (Cy3-P-T) RNA substrate (Marko *et al.* 2013). The RTp66-p51 and RTp66-p66 showed 50–100 times higher affinities for the P-T than the RTp51-p51. Moreover, the RTp51–p51-complex with Cy3-P-T was found to be less stable showing faster dissociation kinetics than the other complexes. The RTp51 has a weak concentration dependence to dimerize, however dimerizes rapidly upon the addition of a non-nucleoside RT inhibitor (NNRTI), Efavirenz (Venezia *et al.* 2006). Another significant experimental observation made was that the unbound/bound ratio of the RTp51 at high concentrations reduced drastically once the NNRTI was added to induce homo-dimerization, indicating dimers have a stronger tendency to bind the Cy3-P-T. Hence, the smPIFE assay indicated a new mechanistic possibility that the dimerization of the RT dictates affinities for substrate interaction.

4.2 *Viral helicase activity measurements*

Single-molecule FRET experiments with HCV NS3 helicase have revealed several interesting features of the viral NS3 helicases (Myong *et al.* 2007). Upon binding of the HCV NS3 helicase in the presence of ATP to initiate dsDNA unwinding, the FRET changes were monitored for dsDNA modified with a donor–acceptor dye pair at the duplex junction. Earlier, force-assisted optical tweezers-based single-molecule detection of NS3 helicase unwinding yielded a characteristic repetitive pattern, in which the helicase would unwind 3–4 bp rapidly followed by long pauses (Dumont *et al.* 2006). The smFRET results indicated six distinct plateaus of FRET decrease for unwinding an 18 bp dsDNA. An automatic step-finding algorithm indicated discrete 3 bp unwinding events, which upon dwell-time analysis revealed hidden 1-bp steps coupled to the hydrolysis of a single ATP molecule per step. At the molecular level, this spring-loaded behaviour was explained by modelling an unwinding process in which domain 3 of the HCV NS3 helicase remains fixed, while domains 1 and 2 translocate and tension is built up in the nucleo-protein complex, which is eventually released in a burst of unwinding activity of three nucleotides (Lin and Kim 1999).

A series of smFRET experiments with NPHII, an SF2 family helicase of the Vaccinia virus, provided interesting

insights to the mechanism of ATPase-coupled RNA unwinding (Fairman-Williams and Jankowsky 2012). Previous studies on NPHII-mediated unwinding indicated that the helicase hydrolyses multiple ATP molecules before initiating strand separation. The inability to decouple distinct conformations upon unwinding was attributed to high ATP turnover numbers (Jankowsky *et al.* 2001). Hence, smFRET experiments were performed using a duplex RNA labelled with a proximal donor–acceptor pair in which the unwinding complex was stalled by various ATP analogs to represent intermediate stages of ATP hydrolysis. Distinct FRET populations corresponding to the unbound RNA and two conformations of bound NPHII to RNA were detected when the ADP-BeFx and ADP-AlFx analogs were titrated; however, the relative ratios of the conformations (FRET states) varied across the two stages of the hydrolysis cycle. In contrast, the ADP-bound NPHII seemed to exclusively prefer an intact duplex to a single-stranded RNA, unlike the ADP-bound state of the HCV NS3. Dwell-time analysis from time trajectories of binding to the non-hydrolyzable ATP analogs revealed multi-phase kinetics of interconversion between the two ssRNA-bound conformational states, indicating a dynamic equilibrium among these NPHII conformations.

Despite the array of studies focusing on the kinetics and mechanism of unwinding by viral helicases, and the emerging role of the NS3 in viral packaging and its translocation, behaviour of helicase on long nucleic acid substrates has not been examined (Dumont *et al.* 2006; Myong *et al.* 2007; Ma *et al.* 2008; Gu and Rice 2010). In a recent study, a hybrid scheme coupling single-molecule fluorescence (TIRFM) with optical tweezers for sub-pixel localization of the helicase in motion on nucleic acids revealed a hitherto unknown interaction phenomenon (Lin *et al.* 2017). The long nucleic acids, maintained as stretched tracks on which fluorescent NS3 helicase molecules can translocate, undergo gradual shortening followed by a force jump and relaxation. This property termed as repetitive translocation was observed exclusively in NS3h–ssDNA interactions, and the shortening rate decreased monotonically with an increase in ssDNA extension force. Furthermore, in an smFRET assay using a partial duplex DNA with a Cy3 donor at the 5' terminus of the longer strand and Cy5 acceptor at the 3' terminus of the shorter strand, the addition of NS3h led to gradual increase in FRET efficiency followed by an abrupt drop. This phenomenon indicated 'repetitive looping' in the DNA, wherein the donor and acceptor strands were periodically brought into proximity over cycles of translocation. A comparison between the translocation rates of NS3 helicase on an ssRNA substrate versus a dsRNA substrate revealed a threefold faster translocation in the former case. This estimate corroborated previous ensemble fluorescence stopped-flow experiments tracking translocation rates of NS3h on polyU and polydU substrates (Khaki *et al.* 2010). This difference can be partially explained by the interaction between the amino acids and the sugar moieties of the nucleic acids in differing conformations, and by the compact structure of ssRNA – a property which decreases the affinity of NS3h.

4.3 *Dynamics of HIV reverse transcriptase on nucleic acid substrates*

Binding to a specific site on the nucleic acid site involves weak binding followed by local search along the length of the polymer, and final reorganization with exploration of multiple alternative configurations of the protein contacts to achieve binding in the 'correct orientation' (Halford and Marko 2004; Blainey *et al.* 2009). In a study conducted by Ganji *et al.* the mechanism of this final reorganization (protein flipping) of the HIV-1 RT on a 19-bp double-primed dsDNA (dpdsDNA) was explored by smFRET. Such protein flipping is a fast event in which the protein moves along a vector perpendicular to the axis of the duplex and specific contacts between the polymerase and nucleic acid duplex are temporarily disrupted and reformed. The RT was observed to bind the symmetric dp duplex DNA in two distinct conformations (exhibiting high and low FRET values of 1 and 0.3 respectively), spending roughly equal times in both conformations but flipping between the two binding states. The dwell time as well as number of binding events of the RT to dpdsDNA was higher at low salt concentrations of 50 nM; at physiologically relevant salt concentrations (150–200 nM) the k_{off} increased and k_{on} decreased. Crowding molecules like PEG 8000, which compact the RT–DNA complex, were found to entropically stabilize the binding. By modelling the effect of macromolecule crowders using the scaled particle theory (Zhou *et al.* 2008), it was shown that at physiological levels of crowding, sub-nanomolar affinities can be achieved for the RT–DNA interactions. Short-range interactions between incoming cognate nucleotides to the RT–DNA complex were found to decrease k_{off} without affecting the P_{flip}, that is, the likelihood of a flipping event versus dissociation from nucleic acid. Using simulations, they demonstrated that a hopping model could describe the long-range interactions under physiological salt and crowding effects to facilitate the RT from rebinding its DNA template. The exploration of multiple configurations between two macromolecules is posited to kinetically aid assembly and function.

A similarly detailed understanding of nucleic acid substrate recognition and polymerization activities of HIV-1 RT was obtained through smFRET-based alternating laser excitation (ALEX) experiments (Liu *et al.* 2008). The HIV-1 RT was labelled with the Cy3 FRET donor on either the RNaseH or the finger domain in the p66 subunit and RNA-DNA hybrids of different lengths were labelled with the acceptor Cy5 dye. FRET histograms with longer hybrid

(38 bp) substrates revealed two distinct binding modes for the interaction: a 'polymerization-competent' mode with the polymerase active site located at the front-end of the hybrid terminus and a 'polymerization-incompetent' mode in which the RNaseH domain is positioned at the back-end of the terminus, based on crystal structures (Jacobo-Molina *et al.* 1993; Sarafianos *et al.* 2001). The distinct FRET values were indicative of the sliding of the HIV-1 RT on the substrate, as the separation of the FRET peaks increases with the length of the RNA–DNA hybrid. Analysis of the FRET signal from a single binding event suggested that the HIV-1 RT shuttles between two ends of the hybrid, a thermally driven diffusion phenomenon. Sliding observed on DNA/DNA duplexes showed higher rate constants for escaping the back-end of the hybrid and lower FRET values accounting for the larger inter-base distance of DNA. The establishment of a kinetic model for sliding of the HIV-1 RT provided significant insights. For example, addition of the initiating nucleotide, dGTP, was found to stabilize the complex of the front-end bound hybrid duplex with HIV-1 RT. In contrast, the NNRTI nevirapine was found to kinetically increase $k_{\text{front}\rightarrow\text{back}}$ by loosening the 'clamp' of the fingers and thumb domains of the RT at the front-end of the hybrid duplex (Huang *et al.* 1998; Quan *et al.* 1998). On long DNA–RNA hybrid tracts, the HIV-RT was found to bind to DNA adjacent to the polymerization site and slide towards the primer terminus, often flipping at the terminus, to achieve the polymerization-competent orientation. These experiments demonstrated that the HIV-1 RT does not adopt a purely one-dimensional search for the polymerization start site, and instead uses sliding and flipping to improve its efficiency.

4.4 *Understanding structure–function relationship in influenza replication*

Influenza A virus has an eight-segment negative-sense single-stranded RNA genome (denoted as vRNA) with complementary regions at the two ends of the genome. The base-pairing between two ends of the RNA genome generates a promoter with a unique structure, a phenomenon similarly proposed for flaviviruses, that enables its RNA-dependent RNA polymerase (RdRP) to recognize the promoter (Robertson 1979; Desselberger *et al.* 1980). In the absence of structural details of the RdRP-bound dsRNA promoter of the influenza A virus, Tomescu *et al.* resorted to single-molecule FRET assay using ALEX to map the structural changes induced in the promoter and dynamics of the interaction with high sensitivity (Kapanidis *et al.* 2005; Tomescu *et al.* 2014). In the first experiment, a synthetic dsRNA promoter was labelled with donor Cy3 at position U18 on the 5′ strand with the acceptor ATTO647N dye at position U4 on the 3′ strand of dsRNA (figure 4a and 4b). The uncorrected mean FRET efficiency (E^*) of the wild-type dsRNA promoter in solution of 0.57 changed on the titration of RdRP with the promoter. The distribution of the RdRP-bound dsRNA promoter complex became bimodal, where the polymerase-bound promoter population had an E^* value of 0.79 (figure 4a). A second smFRET assay was designed to decouple changes between the proximal (residues 1–9) and distal (residues 11–18) promoter changes induced by polymerase binding. In this quenchable smFRET (quFRET) assay (Cordes *et al.* 2010), the proximity of the Cy3 donor dye on residue 3 at the 5′ end and the ATTO647N acceptor dye on U4 at the 3′ end resulted in a quenched low FRET state of the wild-type promoter. The quenching was significantly reversed to a high value of observed FRET ($E^* \sim 0.84$) on titration with RdRP, indicative of opening and rearrangement of the double-helical dsRNA promoter (figure 4b and 4d). To study the structural changes at the distal end, a dsRNA promoter with Cy3 at position 18 on the 5′ end and the ATTO647N dye at position 13 on the 3′ end gave a mean FRET value of $E^* \sim 0.82$, irrespective of RdRP binding, indicating no major structural alteration upon polymerase binding. Structural details were further refined by correcting the E^* values for factors such as background, cross talk and γ-factor effects (to compensate differences in quantum yield and detection efficiency of the fluorophores), to estimate the 'true' donor–acceptor distances. The FRET-restrained positioning and screening, FPS (Kalinin *et al.* 2012) algorithm helped in modelling dyes on the *ab initio* 3D models of the dsRNA promoter in its free and RdRP complexed forms, and was found to be consistent with nuclear magnetic resonance (NMR) structures (figure 4c and 4e). The 3D model generated using corrected FRET efficiencies for the polymerase-bound promoter generated a corkscrew topology as proposed previously (Flick *et al.* 1996). Another key insight from the solution-based assays suggested a dynamic equilibrium between the double-helical and corkscrew conformations. The presence of the corkscrew conformation has been considered significant based on the fact that the hairpin loops are essential for the endonuclease activity of RNAP (Leahy *et al.* 2001a; b) and the polymerase–corkscrew promoter complex is conformationally stable (Brownlee and Sharps 2002). In a similar follow-up study, the promoter was processively unwound during *de novo* replication rather than displaying melting in a single step (Robb *et al.* 2016). The outcome has been a new model for the influenza A replication in which the switch to initiation from its pre-initiation stage is achieved by translocation of the 3' vRNA through the active site, hence destabilizing the processive unwinding the dsRNA promoter.

4.5 *Kinetics of viral IRES-mediated translation*

Translation is a multi-step stochastic process and has been difficult to kinetically understand due to the lack of control over synchronization of ribosomes. Eukaryotic translation has

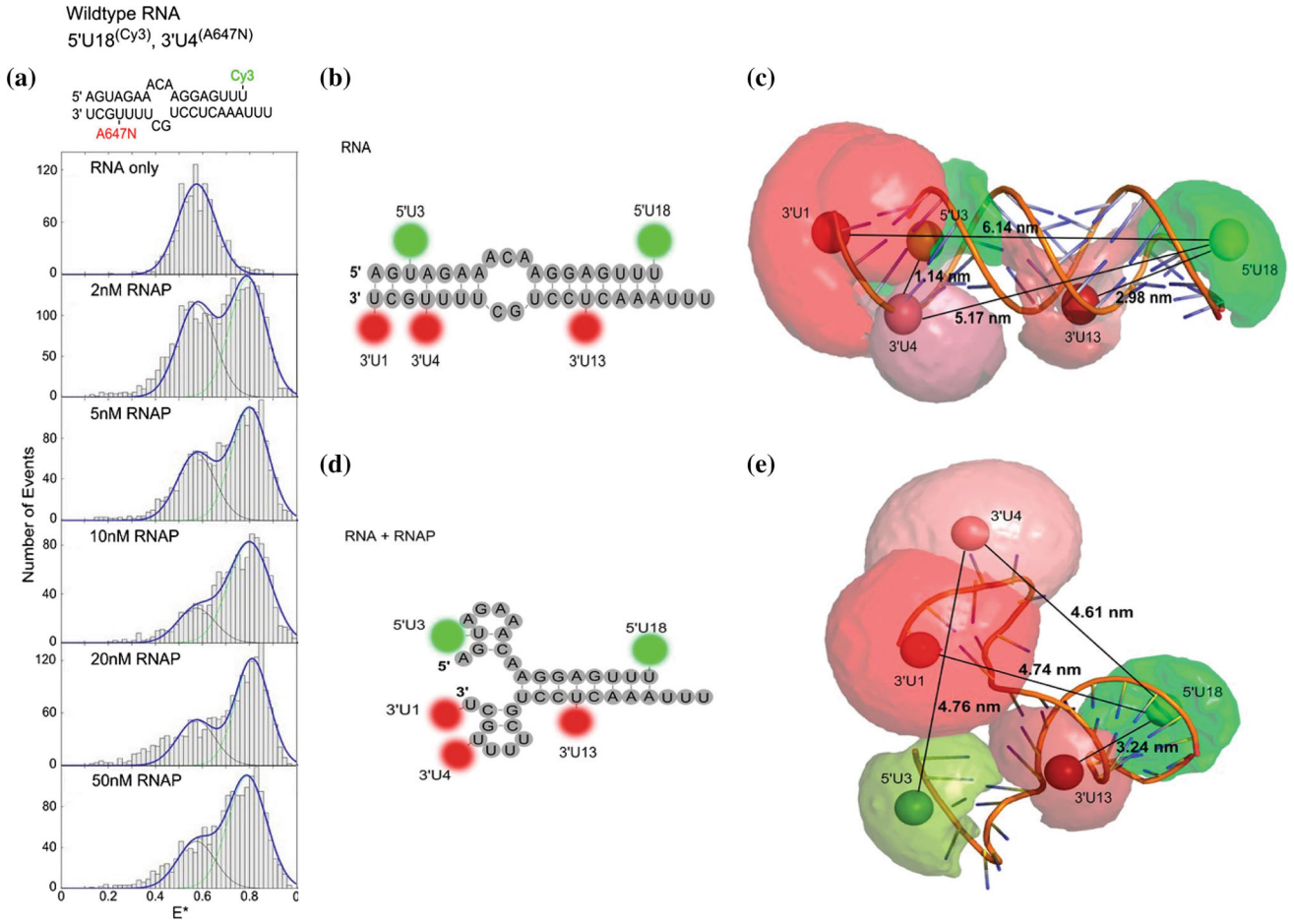

Figure 4. The influenza vRNA promoter adopts a corkscrew structure upon binding by the Influenza A polymerase (Tomescu *et al.* 2014). (**a**) Bimodality in the smFRET distribution upon titrating the vRNA promoter (top panel) with influenza RdRP indicates structural rearrangements in the promoter. (**b**) Representation of the duplex panhandle conformation of the vRNA and alternative labelling sites of the donor (green) and acceptor (red) dyes used to infer distances based on smFRET. (**c**) Three-dimensional (3D) model of the native duplex panhandle vRNA promoter with inter-dye distances indicated. (**d**) Two-dimensional schematic of the expected corkscrew vRNA structure adopted when RdRP opens and restructures the promoter. (**e**) 3D model of the RdRP-bound influenza promoter in the corkscrew configuration. Adapted with permission from The National Academy of Sciences of the USA.

been even more evasive to study by fluorescence due to the complex interactions between the eukaryotic 80S ribosome and its various associated translation factors, the need to incorporate fluorescent labels while minimally perturbing the natural translation system. Sensitive assays for quantifying translation would be informative especially in virology since viruses have evolved multiple strategies for hijacking the host translation machinery. An example of such a strategy is the internal initiation using conserved Internal Ribosome Entry Site (IRES) on viral RNA competent for translation in the host (Firth and Brierley 2012). Bugaud *et al.* tracked how a single mammalian ribosome elongates using the viral IRES, a complex translation initiation sequence (Bugaud *et al.* 2017). Surface-immobilized mRNA (imaged by TIRF microscopy) with either the cricket paralysis virus (CrPV) or the HCV IRES were annealed with two sets of spectrally distinct fluorescent RNA probes at fixed locations from the IRES to report on the translation status (figure 5a). Since the ribosomal entry channel is unable to accommodate double-stranded RNA, the helicase action of the 80S ribosome ensures that the annealed fluorescent probes are unwound as the ribosome translates across the RNA. The placement of the two primers such that one reports on five elongation cycles (+5) and other on nine elongation cycles (+9) post initiation enabled a distinction between initial translation kinetics and elongation kinetics (figure 5b and 5c). A single elongation cycle for CrPV IRES with purified pre-incubated ribosomes was determined to be $\sim 1.4 \pm 0.2$ s, which was slower in comparison with the cycle time of 0.2 s per codon determined by ribosomal profiling (Ingolia *et al.* 2012). An interesting contrast was observed for HCV IRES-mediated translation, which showed a relatively higher efficiency with free ribosomes iterating its

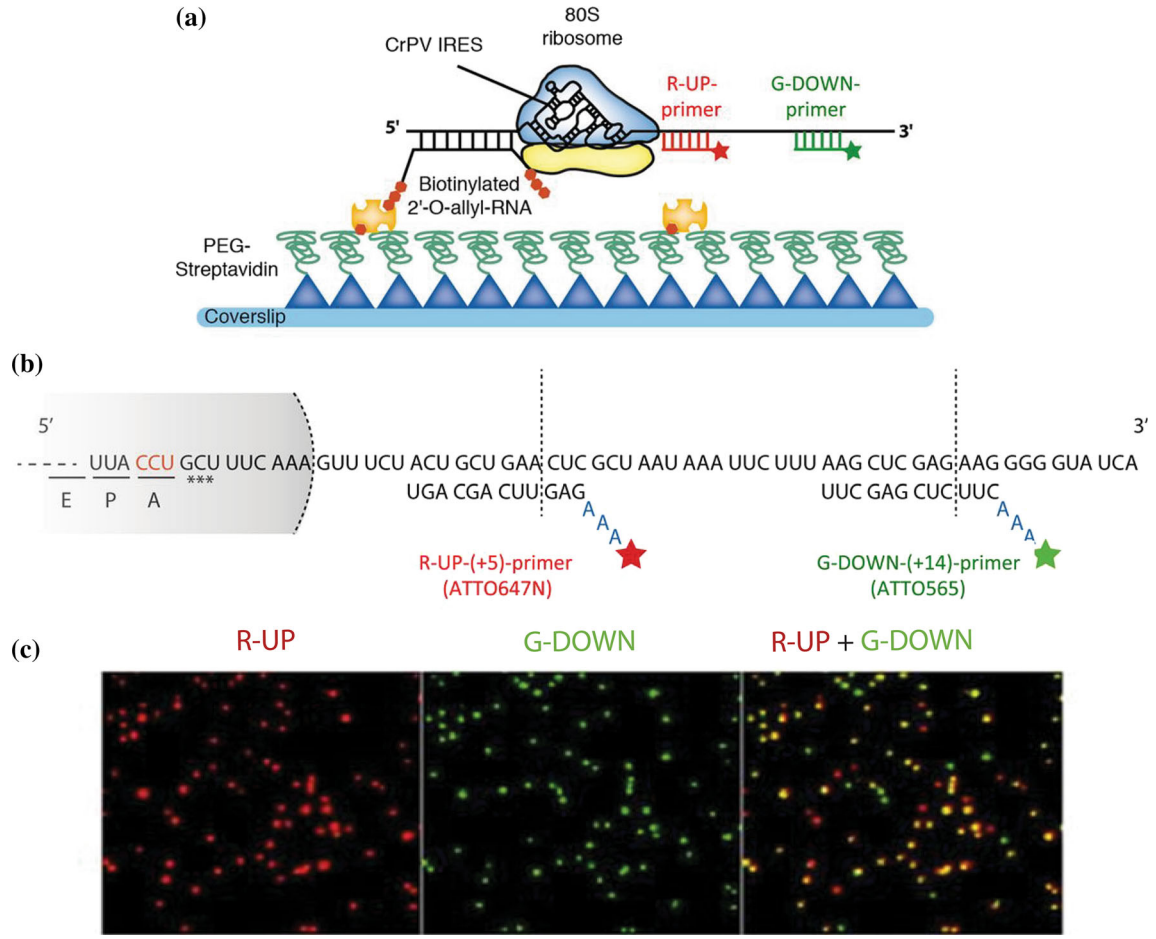

Figure 5. Single ribosome viral IRES translation assay (Bugaud *et al.* 2017). (**a**) A ribosome-bound mRNA is immobilized onto a PEG-neutravidin coverslip through a biotinylated probe complementary to the 5′ end of the mRNA. Each immobilized mRNA is visualized by two hybridized probes, the ATTO647 N UP and ATTO565 DOWN primers. (**b**) Design of the mRNA and fluorescent probes: A-site with the IRES initiator codon is indicated in red; fluorescent probes have three non-complementary nucleotides to act as a spacer between the dye and the mRNA. (**c**) TIRF microscopy images to visualize the co-localization (yellow) of the UP(+5) and DOWN(+14) probes hybridized to each mRNA at the start of the experiment. As translation proceeds, the time difference in probe detachment due to helicase activity of the ribosome can be monitored to estimate translation kinetics. Adapted with the permission of the RNA Society.

dependence on eukaryotic factors like IF2 and IF3 (Borman *et al.* 1995). Furthermore, the distribution of departure times for the (+5) primer could be only fitted to a gamma distribution function with two time parameters indicating different kinetics for intermediate steps. In contrast to studies performed with heterogeneous cell-free translation systems (Zhang *et al.* 2016) where the first four elongation steps were found to be slow (∼80–200 s), CrPV IRES-mediated initiation kinetics was found to be slow in the first two steps (∼40 s) but proceeded more rapidly (∼1.4 s) in subsequent translocation steps. The molecular basis for the appearance of the slower steps may be rationalized by the complex interaction between the ribosome, factor eEF2 and the PKI domain of the CrPV IRES, as studied by cryo-EM (Fernández *et al.* 2014; Murray *et al.* 2016). The ribosome assembles upstream the IRES with an offset of 1 codon, with PKI blocking its A-site. The factor eEF2 interacts with PKI and causes a translocation of the ribosome to correct the offset, the rate-limiting step of translation initiation. Though the A-site is free to accept incoming tRNA, the IRES is shifted to occupy the P- and E-sites, possibly resulting in a second kinetically slow translocation. Once the ribosome translocates beyond the complex IRES, the rest of the elongation steps proceed at a rapid rate. The ribosome assembled on an HCV IRES does not bear an offset (Filbin *et al.* 2012); however, the interactions between the ribosome and the IRES remain like that of CrPV IRES. In addition, the HCV IRES is dependent on multiple initiation factors. A hallmark feature of the IRES-dependent translation as established by these studies is that the first few elongation cycles are rate limiting. This establishes a useful tool to understand translational kinetics and its implications in defining viral fitness in the host.

4.6 *Host–protein interactions with viral RNA in immune response*

Single-molecule fluorescence methods have also found use in probing host factor–viral RNA interactions, a fundamental theme in host immunity to viruses. Viral RNA is initially recognized by pattern recognition receptors (PRRs), and PRRs then induce type I interferons (IFNs) and other pro-inflammatory cytokines, but mechanistic understanding of how viral RNA are discriminated is poor. The Retinoic acid-inducible gene I (RIG-I) is a cytosolic host PRR that provides immunity against many negative-strand RNA viruses by sensing viral RNA (Gack 2014). RIG-I activation occurs only in the presence of pathogenic RNA, despite the ability of RIG-I to bind endogenous RNA in the cytoplasm meriting the question how RIG-I discriminates self- and non-self-RNA. Translocation of the central RNA helicase domain of the RIG-I protein was observed on a dsRNA of a non-viral origin using smPIFE (Myong *et al.* 2009). This truncated RIG-I showed a steady binding to the dsRNA, which changed to periodic fluctuations in fluorescence once ATP was introduced to the protein–RNA complex indicative of repetitive translocation along the length of the dsRNA without unwinding it. A marked dsRNA length and ATP concentration dependence was observed for the translocation of truncated RIG-I, whereas wild-type RIG-I showed low-frequency translocations only. In a splice variant of RIG-I that is incapable of generating antiviral response in the host due to a deficient CARD domain (Gack *et al.* 2008), ATP-dependent translocation on dsRNA resembled that of the truncated RIG-I variant, which was deficient of CARDS. RIG-I displayed larger dwell times on double-stranded RNA/DNA than on ssRNA substrates with 5'triphosphate, which is responsible for activating the ATPase domain of RIG-1 and could be a verification signal for dsRNA to suggest its viral nature. Such a mode of translocation might also assist in removal of RIG-I from low-affinity RNA ligand sites.

5. Viral assembly, packaging and architecture

Viruses must assemble its proteinaceous coat from viral structural proteins, package its genome in it and acquire a lipid membrane encompassing it (if an enveloped virus) in the cytoplasm of the infected cell to generate the virion particles for subsequent infection rounds (Sun *et al.* 2010; Stockley *et al.* 2013; Perlmutter and Hagan 2014; Lakdawala *et al.*2016). This elaborate and extensive process is orchestrated at different locations, time points and through numerous heterogeneous intermediates. Broadly, the virus assembly and packaging progresses through two major pathways. Many single-stranded viruses employ electrostatics and 'packaging' sequences present in their genome to bind capsid (coat) protein and use this nucleation to drive the assembly process while simultaneously packing the genome. On the other hand, when the charge densities and bending flexibility of the nucleic acid set limits on spontaneous assembly, an empty coat shell is pre-assembled and the genome is packaged with the help of devoted nucleic acid motor proteins.

Several single-molecule approaches exist to 'visualize' assembly and packaging of viruses which are reviewed here. While ATP-driven, motor-based packaging of double-stranded nucleic acids into viral procapsid has been studied in detail using single-molecule optical tweezer experiments (Smith 2011), we have limited our discussion to only fluorescence methods for brevity. One fluorescence technique that is sensitive to growth of capsid and that can report on genome packaging without getting overwhelmed by the diversity of intermediates is fluorescence correlation spectroscopy (FCS). FCS relies on detecting mathematical 'likeness' (correlation) in the time scales of fluorescence fluctuations of freely diffusing molecules across a illumination volume (Maiti *et al.* 1997; Ries and Schwille 2012). Since, the time scale of decay for the correlation function is dependent on the diffusion coefficient (which scales with the approximate size) of the particle, virus assembly growth kinetics can be measured in solution (figure 6a). Fluorescently tagged protein, when allowed to assemble *in vitro* or in cells, display increased intensities of particles over time that can be used to track assembly sites and kinetics in real time (figure 6b), though separating single-particle intensities unambiguously becomes challenging in most cases when number of particles per diffraction limited spot goes beyond one. If a singly labelled protein component assembles and can be spatially separated, one can allow irreversible photobleaching of the dyes to estimate the stoichiometry of the assembled complex by counting the number of observed steps in the intensity trace (figure 6c). To determine the identity or number of packaged nucleic acid in the virus, one can use fluorescently labelled complementary oligos (smFISH) that can be hybridized to the nucleic acid in the virion to 'image' the genome (figure 6d).

Finally, the 'super-resolution' avatars of single-molecule imaging like stochastic optical reconstruction microscopy (STORM), photoactivated localization microscopy (PALM) and fluorescence photoactivation localization microscopy (FPALM) are providing new insights regarding virus architecture and its interaction with host cell components. These methods take advantage of image reconstruction from the particle location estimates recovered from mathematical fitting of the point-spread-function of single molecules when induced to stochastically turn-on or undergo photo-blinking (Betzig *et al.* 2006; Hess *et al.* 2006, 'Method of the Year 2008' Nature Methods). We recommend the readers to comprehensive reviews that already cover the developments in this field (Gould and Hess 2008; Ji *et al.* 2008; Hell *et al.*

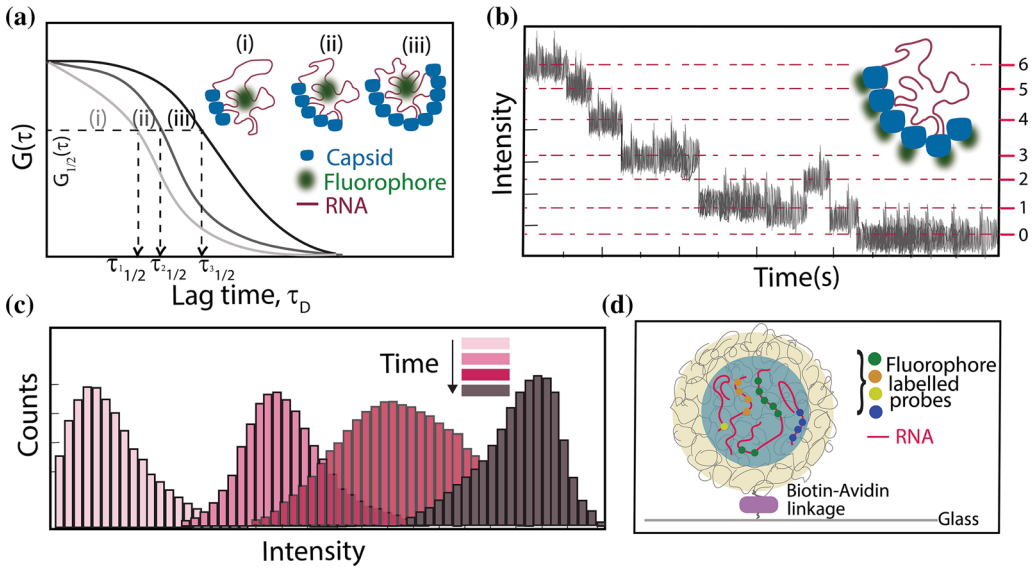

Figure 6. Understanding virus assembly and packaging with fluorescence correlation spectroscopy (FCS), single-molecule fluorescence *in situ* hybridization (smFISH), single-particle photo-bleaching analysis of capsid–RNA complexes. (**a**) Representative auto-correlation functions from fluorescence fluctuations captured in a confocal volume of diffusing molecules can monitor virion assembly. Changes in the hydrodynamic radius of the capsid or the RNA molecule(s) binding is estimated from changes in the diffusion coefficient of the single particles manifesting in decreasing $\tau_{½}$ values. (**b**) Photo-bleaching analysis (in a diffraction-limited spot) of the capsid–nucleic acid complex quantifies the number of labelled capsid protein units enabling examination of the assembly intermediates. The step-wise changes in intensity levels can be directly correlated to the number of labels. (**c**) Fluorescence intensity histograms from single spots depicting time-dependent assembly of capsid protein can report on viral assembly kinetics. As more labelled capsid proteins come together, the intensity of each diffraction-limited spot increases with time. (**d**) Strategy to infer genomic packaging of viruses by smFISH. Fluorophore-labelled FISH probes are designed against different segments of the viral genome and co-localization of probes with virus coat proteins and/or other genome segments allows examination of genome packaging efficiency.

2009; Huang *et al.* 2009; Heilemann 2010; Patterson *et al.* 2010). Compared to electron microscopy, which can reveal exquisite structural detail (at <10 nm), fluorescence super-resolution methods (with lateral resolution of ∼ 10–40 nm) allow access to imaging of multiple species (colour) and dynamical information in physiologically relevant solution conditions. Hence, these methods are already finding applications in understanding of virus architecture, its spatial distribution and organization and its interaction with cellular components that we expect will grow with development of new tools (Müller and Heilemann 2013; Roy 2013; Gray *et al.* 2016) and the information is expected to be significantly enriched in the coming years.

5.1 *Super-resolution microscopy of viruses*

Using photoswitchable fluorescent proteins or photo-blinking dyes tagged to genetic protein fusion tags, various aspects of HIV architecture, assembly and membrane interactions have been extensively studied with super-resolution microscopy (Müller and Heilemann 2013). For example, HIV virion assembly that is coordinated by the virus structural polyprotein Gag on the plasma membrane of the host cell has been studied using Gag's ability to self-assemble into virus-like particles (Betzig *et al.* 2006; Manley *et al.* 2008). Initial stages of Gag assembly was demonstrated to be fast (within 10 min) but proceeded in two phases as a significant (∼ 40%) fraction of the spontaneously forming Gag clusters would be limited to low numbers of Gag proteins (<5% compared to numbers in immature virions) suggesting kinetic barriers to formation of HIV-Gag virions (Ivanchenko *et al.* 2009; Gunzenhäuser *et al.* 2012). Recruitment of HIV Env protein to the Gag clusters could be visualized by co-localization in two-colour super-resolution imaging (Muranyi *et al.* 2013; Roy 2013). Env accumulation was shown to be dependent on direct interaction with the Gag protein, yet it localized to the periphery of the Gag clusters and only low levels of Env were directly associated with the nascent Gag clusters, indicating viral protein-induced restructuring of the membrane composition to assist in virus assembly. Similarly, assembling virus interaction with host cellular proteins can be measured using multi-colour super-resolution imaging. HIV-1 relies on the cellular **e**ndosomal **s**orting **c**omplex **r**equired for **t**ransport (ESCRT) for its final budding step during cell egress. It was previously suggested that ESCRT proteins induced membrane fission from around or below the nascent budding virus. Using

super-resolution microscopy, two groups independently co-localized the ESCRT proteins with Gag protein clusters on the membrane (Van Engelenburg *et al.* 2014; Prescher *et al.* 2015). Both studies demonstrated that when ESCRT proteins did co-localize with the Gag, ESCRT protein clusters were significantly narrower than the HIV-1 bud, suggesting that ESCRT proteins promoted membrane scission inside a narrow structure within the developing bud and did not act from outside. Tetherin, a GPI-anchor membrane cellular restriction factor that is known to inhibit the release of enveloped viruses, was shown to co-localize to HIV assembly sites (Lehmann *et al.* 2011). Tetherin clustering was mediated by the transmembrane domain interactions but was not associated with lipid raft domains unlike popular belief, and it likely tethered the developing HIV-1 virions directly to the plasma membrane, suggesting the mechanistic basis for tetherin inhibition of viral action. Stimulated emission depletion (STED)-based super-resolution microscopy has also aided in understanding of the HIV maturation process. Using dual-colour STED, Stefan Hell's group demonstrated maturation of the HIV-1 virion was associated with rearrangement and clustering of Env proteins close to the cluster of receptor molecules (Chojnacki *et al.* 2012). This has led to the emergence of the idea that Gag maturation signalling primes the onset of events necessary for cell entry and post-entry events. Using photo-cleavage of an HIV maturation inhibitor, time-resolved induction of Gag polyprotein cleavage and virion protein relocalization was studied in a synchronized fashion allowing direct visualization of the virus maturation at the sub-viral level over the course of tens of minutes (Hanne *et al.* 2016). We predict that such sub-viral resolution afforded by fluorescence super-resolution techniques will be employed increasingly to understand virus processes in the future.

5.2 *Single-molecule FISH to study viral RNA lifecycle and genome packaging*

Using single-molecule RNA (sm)FISH against Influenza genome, it was shown that virus packages its segmented genome at one copy per RNA segment per viral particle (Chou *et al.* 2012). The mechanism for such precise single-copy packaging of each segment was further revealed to be orchestrated in the cytoplasm itself. When the viral genome segments were observed with two-colour single-molecule FISH, co-localized signals for genome segments revealed that the viral RNA was transported collectively to the nucleus post infection (Chou *et al.* 2013). The newly replicated viral RNA would then be distributed spatially in the cell cytoplasm but would start to reassemble with its counterparts in Rab11-enriched recycling endosomes. On the other hand, smFISH with the Rift valley Fever virus, a bunya virus that carries a tripartite RNA genome showed the absence of one or more genomic segments in the virus particles, indicating that RVFV packaging was a non-selective process (Wichgers Schreur and Kortekaas 2016). Interestingly, RVFV RNA imaged in the cells post infection showed how the virus would start replicating locally at the site of infection, then spread to cytoplasm, before being localized at the Golgi with the help of Gn glycoprotein.

Similar studies in combination with immuno-fluorescence employed in case of LCMV has also revealed how genome replication and pre-assembly would take place in Rab5c early endosomes (King *et al.* 2017). In HCV cell infection model, smFISH against the positive and negative strands of the viral RNA and their simultaneous imaging with ribosomes and viral proteins highlighted the dynamics of HCV lifecycle (Shulla and Randall 2015). Positive strands of the viral RNA were initially associated with the ribosomes but over time co-localized with virus 'replication factories' and finally virus assembly highlighting the spatio-temporal regulation of the viral RNA. Extending this approach, Ramanan *et al.* examined the effect of various antivirals on HCV viral dynamics (Ramanan *et al.* 2016). HCV antivirals displayed strand-specific decay kinetics suggesting differences in underlying mechanism of these drugs. For example, daclatasvir (DCV) treatment led to early dramatic drops in negative strand of vRNA, while IFN treatment produced a much weaker and variable response per cell. Intriguingly, IFN induction of interferon-stimulated genes (ISGs) that are known to play a role in suppression of vRNA was not only highly variable among cells, but also their RNA levels were positively correlated with viral RNA levels. Such quantitative single genome measurements in single cells allow an unprecedented level of accuracy that combined with kinetic modelling of virus lifecycles can provide crucial insights into virus–host cell interactions.

5.3 *Virus assembly in vitro*

Virus particles can be assembled *in vitro* from the coat proteins with and without the genome in optimized solution salt conditions (Zlotnick and Mukhopadhyay 2011; Bush and Vogt 2014). This, combined with lack of specific sequences shown to be associated with virus assembly, has led to the widely held belief that viral coat assembly is largely driven by electrostatics. However, most of such *in vitro* assemblies must rely on high protein concentrations ($\sim$ 1–10 μM), require long incubations and sample processing and purification to observe the assembled structures. In the cells, viral genome is able to compete with high concentrations of cellular RNA and is present exclusively in the mature virions (Routh *et al.* 2012). This has led to the search for virus assembly packaging principles that can explain this crucial aspect of its lifecycle. Since the virus assembly *in vivo* and in the initial stages occurs with sub-micromolar

concentrations of coat proteins, Peter Stockley's group adapted FCS to monitor assembly of virus particles in real time (Borodavka *et al.* 2012). FCS reports on the diffusion coefficient of the tagged molecule (either the RNA or the coat protein) which can be employed to determine the hydrodynamic radii (R_h) of the growing virus particle with time. Using two distinct ssRNA viruses, they showed that addition of capsid proteins to the labelled RNA would result in a rapid and dramatic condensation of the RNA (drop of $\sim$ 20–30% of R_h). The capsid–RNA complex would then grow to resemble the size of fully formed viruses. Non-viral RNA would not display any such changes and produced only aberrant structures, suggesting that specific interaction between viral RNA and capsid was important for virus assembly. Interestingly, the RNA collapse also required inter-protein interactions, indicating that capsid assembly was being nucleated. Based on this, they proposed a two-stage mechanism for virus assembly: (i) a rapid and cooperative capsid binding at multiple 'high' nanomolar affinity locations on the RNA and compaction of the RNA by capsid–capsid interactions and (ii) addition of capsid proteins to this nucleoprotein complex. In a more recent study, they attempted to 'redesign' the assembly process using mutations of the RNA sites involved in capsid binding, that is, 'packaging signals (PS)' on the viral genome (Patel *et al.* 2017). Virion formation was compromised when all such capsid recognition motifs were removed from the viral RNA. Working with a smaller RNA region and introducing synthetic motifs that bind tightly to the capsid, they could restore assembly of the PS-less RNA or generate more efficient assembling genomes that could outcompete the wild-type genome. Such increased understanding of virus assembly can help in design and development of better vaccines, gene therapy carriers and aid in search of antivirals that target the viral assembly process.

6. Challenges and outlook for the future

In spite of its potential for revealing fresh insights into biomolecular systems, single-molecule methods have found limited adoption in virology and even in the biology scientific community. Apart from costs of initial investment on setups, the complexities in developing single-molecule assays requires a broad understanding of issues with sample preparation, limitations of the methods and challenges in data interpretation. Availability of integrated optical microscope systems and possible service-based business models that have helped genomics and proteomics approaches could alleviate some of the issues. Other technical issues are addressable but working closely or visiting operating labs in the field can help alleviate initial hiccups and learning-curve bottlenecks.

We expect several other technical innovations will drive progress in application of single-molecule fluorescence in virology and other areas. One of the common challenges in conducting single-molecule fluorescence experiments still remains to be shortage of fluorescently tagged biological reagents. Due to the demand for high photon flux, high photostability, genetic and/or orthogonal bioconjugation, single-molecule fluorescence probes are far and few and further development in this area will fuel increase in single-molecule applications. Currently, single-protein labelling with Cyanine, ATTO and Alexa family of organic dyes remain popular. Genetic tagging with fluorescent proteins like EYFP and RFP is employed though they suffer from lower photon budget and controlling their expression levels to get optimal density of molecules for single-molecule imaging is challenging. Photoswitchable and photoactivable proteins like mEOS2 and PA-GFP provide a better handle on managing the number of observable molecules due to control over the activation process. Self-labelling protein tags like SNAP-tag and Halo-tag provide an opportunity to use the photon budget of dyes with genetic encoding (Keppler *et al.* 2003; Los *et al.* 2008). Similarly, improved methods that label the viral nucleic acid at high signal-to-noise ratio with help of nucleic acid tags such as nuclease-resistant molecular beacons, GFP fusion proteins that bind to RNA/DNA secondary structure and/or multiply labelled tetravalent RNA imaging probes (MTRIPs) will help enhance virus tracking and cell-entry (Sivaraman *et al.* 2011; Alonas *et al.* 2016). Apart from development of new fluorophores, ways to conjugate smaller variants of Q-dots and other promising candidates like nitrogen-vacancy centres in diamond can provide photostable and high-contrast alternatives to dyes, especially for rapid tracking and long-term imaging. Convenience of introducing these tags also require plasmid-based cDNA infectious clones to enable straightforward molecular biology and purification, high-throughput ways of measuring activity and viability after tagging, and convenient methods for delivery of tagged molecules to cells.

However, advances in illumination and imaging schemes that provide advantages of enhanced signal-to-noise ratio, higher imaging speeds with wide-field imaging and better optical-sectioning for 3D imaging are already demonstrating promise (Gebhardt *et al.* 2013; Chen *et al.* 2014; Greiss *et al.* 2016). Parallel development of analytical tools and algorithms, tracking of fluorescent particles, stoichiometry analysis of molecular complexes and recovery of physical properties like diffusional and structural dynamics are expected to percolate and become 'standards' for single-molecule data analysis pipelines (McKinney *et al.* 2006; Greenfeld *et al.* 2012; Persson *et al.* 2013; Coltharp *et al.* 2014; Gray *et al.* 2016).

Another front for further development will be a combination of single-molecule fluorescence imaging with other non-fluorescence-based imaging and spectroscopy platforms that can enhance the informational output of the single-molecule assays. *In vitro* mechanical manipulation methods

like optical and magnetic tweezers, atomic force microscopy (Neuman and Nagy 2008) and acoustic force spectroscopy (Kamsma *et al.* 2016) that can apply pN to nN range of forces on single molecules have already been combined with fluorescence detection (Zhou *et al.* 2010; Kemmerich *et al.* 2016). Apart from aiding in understanding of virus–receptor interactions (Alsteens *et al.* 2016) and mechano-chemical coupling of viral enzymes (Dumont *et al.* 2006; Cheng *et al.* 2011; Lin and Ha 2017), these methods can allow mapping of the cellular mechanics upon infection (Grashoff *et al.* 2010). Other high-throughput global analysis approaches like genomics and proteomics, when coupled to single-molecule methods, are finding use in evaluating the cell-to-cell heterogeneity and can become powerful tools in addressing stochasticity in viral infection and host-response (Lubeck and Cai 2012; Lovatt *et al.* 2014; Lee *et al.* 2015; Moffitt *et al.* 2016).

Single-molecule experiments have also remained largely *in vitro* in nature with studies primarily employing recombinant and truncated versions of the viral components to enable easy and 'correct' interpretation of data. Generation of single-molecule experiment capable of constructs using genetic approaches (Nelles *et al.* 2016; Khan *et al.* 2017), ability to visualize single molecules deep in animal tissue (Chen *et al.* 2014; Greiss *et al.* 2016; Shah *et al.* 2016), automation and increased user-friendliness of single molecule experiments (necessary for adaptation to enhanced biosafety level facilities) can increase the impact of single-molecule-based methods in virology and other infectious diseases.

Acknowledgements

This work was supported by Indian Institute of Science (IISc) Bangalore, Wellcome Trust—DBT India Alliance Intermediate fellowship and Department of Biotechnology-Innovative Young Biotechnologist Award to RR. We also thank Vaseef Rizvi and Lakshmi Supriya for carefully reading the manuscript.

References

Alonas E, Vanover D, Blanchard E, Zurla C and Santangelo PJ 2016 Imaging viral RNA using multiply labeled tetravalent RNA imaging probes in live cells. *Methods* **98** 91–98

Alsteens D, Newton R, Schubert R, Martinez-Martin D, Delguste M, Roska B and Müller DJ 2016 Nanomechanical mapping of first binding steps of a virus to animal cells. *Nature Nanotechnology* **12** 177–183

Avilov SV, Moisy D, Naffakh N and Cusack S 2012 Influenza A virus progeny vRNP trafficking in live infected cells studied with the virus-encoded fluorescently tagged PB2 protein. *Vaccine* **30** 7411–7417

Axelrod D 1981 Cell-substrate contacts illuminated by total internal reflection fluorescence. *J. Cell Biol.* **89** 141–145

Betzig E, Patterson GH, Sougrat R, Lindwasser OW, Olenych S, Bonifacino JS, Davidson MW, Lippincott-Schwartz J and Hess HF 2006 Imaging intracellular fluorescent proteins at nanometer resolution. *Science* **313** 1642–1645

Blainey PC, Luo G, Kou SC, Mangel WF, Verdine GL, Bagchi B and Xie XS 2009 Nonspecifically bound proteins spin while diffusing along DNA. *Nat Struct Mol Biol.* **16** 1224–1229

Blumenthal R, Durell S and Viard M 2012 HIV entry and envelope glycoprotein-mediated fusion. *J. Biol. Chem.* **287** 40841–40849

Borman AM, Bailly JL, Girard M and Kean KM 1995 Picornavirus internal ribosome entry segments: comparison of translation efficiency and the requirements for optimal internal initiation of translation in vitro. *Nucleic Acids Res.* **23** 3656–3663

Borodavka A, Tuma R and Stockley PG 2012 Evidence that viral RNAs have evolved for efficient, two-stage packaging. *Proc Natl Acad Sci USA* **109** 15769–15774

Brandenburg B, Lee LY, Lakadamyali M, Rust MJ, Zhuang X and Hogle JM 2007 Imaging poliovirus entry in live cells. *PLoS Biology* **5** 1543–1555

Brandenburg B and Zhuang X 2007 Virus trafficking - Learning from single-virus tracking. *Nat Rev Microbiol* **5** 197–208

Brownlee GG and Sharps JL 2002 The RNA polymerase of influenza a virus is stabilized by interaction with its viral RNA promoter. *J Virol.* **76** 7103–7113

Bugaud O, Barbier N, Chommy H, Fiszman N, Le Gall A, Dulin D, Saguy M, Westbrook N, Perronet K and Namy O 2017 Kinetics of CrPV and HCV IRES-mediated eukaryotic translation using single-molecule fluorescence microscopy. *RNA* **23** 1626–1635

Bush DL and Vogt VM 2014 In Vitro Assembly of Retroviruses. *Annu. Rev. Microbiol.* **1** 561–580

Chao LH, Klein DE, Schmidt AG, Peña JM and Harrison SC 2014 Sequential conformational rearrangements in flavivirus membrane fusion. *eLife* **3** e04389

Chen BC, Legant WR, Wang K, Shao L, Milkie DE, Davidson MW, Janetopoulos C, Wu XS, Hammer JA, Liu Z, English BP, Mimori-Kiyosue Y, Romero DP, Ritter AT, Lippincott-Schwartz J, Fritz-Laylin L, Mullins RD, Mitchell DM, Bembenek JN, Reymann AC, Böhme R, Grill SW, Wang JT, Seydoux G, Tulu US, Kiehart DP and Betzig E 2014 Lattice light-sheet microscopy: Imaging molecules to embryos at high spatiotemporal resolution. *Science* **346** 1257998

Cheng W, Arunajadai SG, Moffitt JR, Tinoco I and Bustamante C 2011 Single-base pair unwinding and asynchronous RNA release by the Hepatitis C virus NS3 helicase. *Science* **333** 1746–1749

Chernomordik LV and Kozlov MM 2003 Protein–lipid interplay in fusion and fission of biological membranes. *Annu. Rev. Biochem.* **72** 175–207

Chojnacki J, Staudt T, Glass B, Bingen P, Engelhardt J, Anders M, Schneider J, Müller B, Hell S W and Kräusslich HG 2012 Maturation-dependent HIV-1 surface protein redistribution revealed by fluorescence nanoscopy. *Science* **338** 524–528

Chou Y, Vafabakhsh R, Doğanay S, Gao Q, Ha T and Palese P 2012 One influenza virus particle packages eight unique viral RNAs as shown by FISH analysis. *Proc Natl Acad Sci USA* **109** 9101–9106

Chou Y Ying, Heaton NS, Gao Q, Palese P, Singer R and Lionnet T 2013 Colocalization of different influenza viral RNA segments in the cytoplasm before viral budding as shown by single-molecule sensitivity FISH analysis. *PLoS Pathogens* **9** e1003358

Coltharp C, Yang X and Xiao J 2014 Quantitative analysis of single-molecule superresolution images. *Curr Opin Struct Biol.* **28** 112–121

Cordes T, Santoso Y, Tomescu AI, Gryte K, Hwang LC, Camará B, Wigneshweraraj S and Kapanidis AN 2010 Sensing DNA opening in transcription using quenchable Förster resonance energy transfer. *Biochemistry* **49** 9171–9180

Costello DA, Lee DW, Drewes J, Vasquez KA, Kisler K, Wiesner U, Pollack L, Whittaker GR and Daniel S 2012 Influenza virus-membrane fusion triggered by proton uncaging for single particle studies of fusion kinetics. *Anal. Chem.* **84** 8480–8489

Costello DA, Millet JK, Hsia CY, Whittaker GR and Daniel S 2013 Single particle assay of coronavirus membrane fusion with proteinaceous receptor-embedded supported bilayers. *Biomaterials* **34** 7895–7904

Coyne CB and Bergelson JM 2006 Virus-induced Abl and Fyn kinase signals permit coxsackievirus entry through epithelial tight junctions. *Cell* **124** 119–131

Daly TJ, Doten RC, Rennert P, Auer M, Jaksche H, Donner A, Fisk G and Rusche JR 1993 Biochemical characterization of binding of multiple HIV-1 Rev monomeric proteins to the Rev responsive element. *Biochemistry* **32** 10497–10505

Desselberger U, Racaniello VR, Zazra JJ and Palese P 1980 The 3' and 5'-terminal sequences of influenza A, B and C virus RNA segments are highly conserved and show partial inverted complementarity. *Gene* **8** 315–328

Dumont S, Cheng W, Serebrov V, Beran RK, Tinoco I, Pyle AM and Bustamante C 2006 RNA translocation and unwinding mechanism of HCV NS3 helicase and its coordination by ATP. *Nature* **439** 105–108

Van Engelenburg SB, Shtengel G, Sengupta P, Waki K, Jarnik M, Ablan SD, Freed EO, Hess HF and Lippincott-Schwartz J 2014 Distribution of ESCRT machinery at HIV assembly sites reveals virus scaffolding of ESCRT subunits. *Science* **343** 653–656

Fairman-Williams ME and Jankowsky E 2012 Unwinding initiation by the viral RNA helicase NPH-II. *J. Mol. Biol.* **415** 819–832

Fernández IS, Bai X-C, Murshudov G, Scheres SHW and Ramakrishnan V 2014 Initiation of translation by cricket paralysis virus IRES requires its translocation in the ribosome. *Cell* **157** 823–831

Filbin ME, Vollmar BS, Shi D, Gonen T and Kieft JS 2012 HCV IRES manipulates the ribosome to promote the switch from translation initiation to elongation. *Nat. Struct. Mol. Biol.* **20** 150–158

Finco O and Rappuoli R 2014 Designing vaccines for the twenty-first century society. *Front. Immunol.* **5** 12

Finke S, Brzózka K and Conzelmann K-K 2004 Tracking fluorescence-labeled rabies virus: enhanced green fluorescent protein-tagged phosphoprotein P supports virus gene expression and formation of infectious particles. *J. Virol.* **78** 12333–12343

Firth AE and Brierley I 2012 Non-canonical translation in RNA viruses. *J. Gen. Virol.* **93** 1385–1409

Flick R, Neumann G, Hoffmann E, Neumeier E and Hobom G 1996 Promoter elements in the influenza vRNA terminal structure. *RNA* **2** 1046–1057

Floyd DL, Ragains JR, Skehel JJ, Harrison SC and van Oijen AM 2008 Single-particle kinetics of influenza virus membrane fusion. *Proc Natl Acad. Sci.* **105** 15382–15387

Gack MU 2014 Mechanisms of RIG-I-like receptor activation and manipulation by viral pathogens. *J. Virol.* **88** 5213–5216

Gack MU, Kirchhofer A, Shin YC, Inn K-S, Liang C, Cui S, Myong S, Ha T, Hopfner K-P and Jung JU 2008 Roles of RIG-I N-terminal tandem CARD and splice variant in TRIM25-mediated antiviral signal transduction. *Proc. Natl. Acad. Sci. USA* **105** 16743–16748

Gebhardt JCM, Suter DM, Roy R, Zhao ZW, Chapman AR, Basu S, Maniatis T and Xie XS 2013 Single-molecule imaging of transcription factor binding to DNA in live mammalian cells. *Nat. Methods* **10** 421–426

Gould TJ and Hess ST 2008 Nanoscale biological fluorescence imaging. *Methods Cell Biol.* **89** 329–358

Granstedt AE, Brunton BW and Enquist LW 2013 Imaging the transport dynamics of single alphaherpesvirus particles in intact peripheral nervous system explants from infected mice. *mBio* **4** e00358-13–e00358-13

Grashoff C, Hoffman BD, Brenner MD, Zhou R, Parsons M, Yang MT, McLean MA, Sligar SG, Chen CS, Ha T and Schwartz MA 2010 Measuring mechanical tension across vinculin reveals regulation of focal adhesion dynamics. *Nature* **466** 263–266

Gray RDM, Beerli C, Pereira PM, Scherer KM, Samolej J, Bleck CKE, Mercer J and Henriques R 2016 VirusMapper: open-source nanoscale mapping of viral architecture through super-resolution microscopy. *Sci. Rep.* **6** 29132

Greenfeld M, Pavlichin DS, Mabuchi H and Herschlag D 2012 Single molecule analysis research tool (SMART): An integrated approach for analyzing single molecule data. *PLoS ONE* **7** e30024

Greiss F, Deligiannaki M, Jung C, Gaul U and Braun D 2016 Single-molecule imaging in living drosophila embryos with reflected light-sheet microscopy. *Biophys. J.* **110** 939–946

Le Grice SF and Grüninger-Leitch F 1990 Rapid purification of homodimer and heterodimer HIV-1 reverse transcriptase by metal chelate affinity chromatography. *Eur. J. Biochem.* **187** 307–314

Gu M and Rice CM 2010 Three conformational snapshots of the hepatitis C virus NS3 helicase reveal a ratchet translocation mechanism. *Proc. Natl. Acad. Sci.* **107** 521–528

Gunzenhäuser J, Olivier N, Pengo T and Manley S 2012 Quantitative super-resolution imaging reveals protein stoichiometry and nanoscale morphology of assembling HIV-gag virions. *Nano Lett.* **12** 4705–4710

Halford SE and Marko JF 2004 How do site-specific DNA-binding proteins find their targets? *Nucleic Acids Res.* **32** 3040–3052

Hanne J, Göttfert F, Schimer J, Anders-Össwein M, Konvalinka J, Engelhardt J, Müller B, Hell SW and Kräusslich, HG 2016 Stimulated emission depletion nanoscopy reveals time-course of human immunodeficiency virus proteolytic maturation. *ACS Nano* **10** 8215–8222

Harrison SC 2008 Viral membrane fusion. *Nat. Struct. Mol. Biol.* **15** 690–698

Harrison SC 2015 Viral membrane fusion. *Virology* **479–480** 498–507

Heilemann M 2010 Fluorescence microscopy beyond the diffraction limit. *J. Biotechnol.* **149** 243–251

Heldt FS, Kupke SY, Dorl S, Reichl U and Frensing T 2015 Single-cell analysis and stochastic modelling unveil large cell-to-cell variability in influenza A virus infection. *Nat. Commun.* **6** 8939

Hell SW, Schmidt R and Egner A 2009 Diffraction-unlimited three-dimensional optical nanoscopy with opposing lenses. *Nat. Photonics* **3** 381–387

Hess ST, Girirajan TPK and Mason MD 2006 Ultra-high resolution imaging by fluorescence photoactivation localization microscopy. *Biophys. J.* **91** 4258–4272

Hoornweg TE, van Duijl-Richter MKS, Ayala Nuñez NV, Albulescu IC, van Hemert MJ and Smit JM 2016 Dynamics of chikungunya virus cell entry unraveled by single virus tracking in living cells. *J. Virol.* **90** JVI.03184-15

Howard CR and Fletcher NF 2012 Emerging virus diseases: can we ever expect the unexpected? *Emerg. Microbes Infect.* **1** e46–e46

Huang B, Bates M and Zhuang X 2009 Super-resolution fluorescence microscopy. *Annu. Rev. Biochem.* **78** 993–1016

Huang H, Chopra R, Verdine GL and Harrison SC 1998 Structure of a covalently trapped catalytic complex of HIV-1 reverse transcriptase: implications for drug resistance. *Science* **282** 1669–1675

Hwang H and Myong S 2014 Protein induced fluorescence enhancement (PIFE) for probing protein-nucleic acid interactions. *Chem. Soc. Rev.* **43** 1221–1229

Ingolia NT, Brar GA, Rouskin S, McGeachy AM and Weissman JS 2012 The ribosome profiling strategy for monitoring translation in vivo by deep sequencing of ribosome-protected mRNA fragments. *Nat. Protoc.* **7** 1534–1550

Ivanchenko S, Godinez WJ, Lampe M, Krusslich HG, Eils R, Rohr K, Bruchle C, Muller B and Lamb DC 2009 Dynamics of HIV-1 assembly and release. *PLoS Pathogens* **5** e1000652

Ivanovic T, Choi JL, Whelan SP, van Oijen AM and Harrison SC 2013 Influenza-virus membrane fusion by cooperative fold-back of stochastically induced hemagglutinin intermediates. *eLife* **2013** 1–20

Jacobo-Molina A, Ding J, Nanni RG, Clark AD, Lu X, Tantillo C, Williams RL, Kamer G, Ferris AL and Clark P 1993 Crystal structure of human immunodeficiency virus type 1 reverse transcriptase complexed with double-stranded DNA at 3.0 A resolution shows bent DNA. *Proc. Natl. Acad. Sci. USA* **90** 6320–6324

Jankowsky E, Gross CH, Shuman S and Pyle AM 2001 Active disruption of an RNA-protein interaction by a DExH/D RNA helicase. *Science* **291** 121–125

Ji N, Shroff H, Zhong H and Betzig E 2008 Advances in the speed and resolution of light microscopy. *Curr. Opin. Neurobiol.* **18** 605–616

Jones KE, Patel NG, Levy MA, Storeygard A, Balk D, Gittleman JL and Daszak P 2008 Global trends in emerging infectious diseases. *Nature* **451** 990–993

Joo C, Balci H, Ishitsuka Y, Buranachai C and Ha T 2008 Advances in single-molecule fluorescence methods for molecular biology. *Annu. Rev. Biochem.* **77** 51–76

Kalinin S, Peulen T, Sindbert S, Rothwell PJ, Berger S, Restle T, Goody RS, Gohlke H and Seidel CAM 2012 A toolkit and benchmark study for FRET-restrained high-precision structural modeling. *Nat. Methods* **9** 1218–1225

Kamsma D, Creyghton R, Sitters G, Wuite GJL and Peterman EJG 2016 Tuning the music: acoustic force spectroscopy (AFS) 2.0. *Methods* **105** 26–33

Kapanidis AN, Laurence TA, Lee NK, Margeat E, Kong X and Weiss S 2005 Alternating-laser excitation of single molecules. *Accounts Chem. Res.* **38** 523–533

Kemmerich FE, Swoboda M, Kauert DJ, Grieb MS, Hahn S, Schwarz FW, Seidel R and Schlierf M 2016 Simultaneous single-molecule force and fluorescence sampling of dna nanostructure conformations using magnetic tweezers. *Nano Lett.* **16** 381–386

Keppler A, Gendreizig S, Gronemeyer T, Pick H, Vogel H and Johnsson K 2003 A general method for the covalent labeling of fusion proteins with small molecules in vivo. *Nature Biotechnol.* **21** 86–89

Khaki AR, Field C, Malik S, Niedziela-Majka A, Leavitt SA, Wang R, Hung M, Sakowicz R, Brendza KM and Fischer CJ 2010 The macroscopic rate of nucleic acid translocation by Hepatitis C virus helicase NS3h is dependent on both sugar and base moieties. *J. Mol. Biol.* **400** 354–378

Khan AO, Simms VA, Pike JA, Thomas SG and Morgan NV 2017 CRISPR-Cas9 mediated labelling allows for single molecule imaging and resolution. *Sci. Rep.* **7** 8450

King BR, Kellner S, Eisenhauer PL, Bruce EA, Ziegler CM, Zenklusen D and Botten JW 2017 Visualization of the lymphocytic choriomeningitis mammarenavirus (LCMV) genome reveals the early endosome as a possible site for genome replication and viral particle pre-assembly. *J. Gen. Virol.* **98** 2454

Kobiler O, Brodersen P, Taylor MP, Ludmir EB and Enquist LW 2011 Herpesvirus replication compartments originate with single incoming viral genomes. *mBio* **2** e00278-11

Koh HR, Wang X and Myong S 2016 Visualizing repetitive diffusion activity of double-strand RNA binding proteins by single molecule fluorescence assays. *Methods* **105** 109–118

Kohlstaedt LA, Wang J, Friedman JM, Rice PA and Steitz TA 1992 Crystal structure at 3.5 A resolution of HIV-1 reverse transcriptase complexed with an inhibitor. *Science* **256** 1783–90

Kukura P, Ewers H, Müller C, Renn A, Helenius A and Sandoghdar V 2009 High-speed nanoscopic tracking of the position and orientation of a single virus. *Nat. Methods* **6** 923–927

Lakadamyali M, Rust MJ, Babcock HP and Zhuang X 2003 Visualizing infection of individual influenza viruses. *Proc. Natl. Acad. Sci.* **100** 9280–9285

Lakadamyali M, Rust MJ and Zhuang X 2006 Ligands for clathrin-mediated endocytosis are differentially sorted into distinct populations of early endosomes. *Cell* **124** 997–1009

Lakdawala SS, Fodor E and Subbarao K 2016 Moving on out: transport and packaging of influenza viral rna into virions. *Annu. Rev. Virol.* **3** 411–427

Lamichhane R, Hammond JA, Pauszek RF, Anderson RM, Pedron I, van der Schans E, Williamson JR and Millar DP 2017 A DEAD-box protein acts through RNA to promote HIV-1 Rev-RRE assembly. *Nucleic Acids Res.* **45** 4632–4641

Leahy MB, Dobbyn HC and Brownlee GG 2001 Hairpin loop structure in the 3 arm of the influenza A virus virion RNA promoter is required for endonuclease activity. *J. Virol.* **75** 7042–7049

Leahy MB, Pritlove DC, Poon LL and Brownlee GG 2001 Mutagenic analysis of the 5' arm of the influenza A virus virion RNA promoter defines the sequence requirements for endonuclease activity. *J. Virol.* **75** 134–42

Lee JH, Daugharthy ER, Scheiman J, Kalhor R, Ferrante TC, Terry R, Turczyk BM, Yang JL, Lee HS, Aach J, Zhang K and Church GM 2015 Fluorescent in situ sequencing (FISSEQ) of RNA for gene expression profiling in intact cells and tissues. *Nat. Protoc.* **10** 442–458

Lehmann MJ, Sherer NM, Marks CB, Pypaert M and Mothes W 2005 Actin- and myosin-driven movement of viruses along filopodia precedes their entry into cells. *J. Cell Biol.* **170** 317–325

Lehmann M, Rocha S, Mangeat B, Blanchet F, Uji-i H, Hofkens J and Piguet V 2011 Quantitative multicolor super-resolution microscopy reveals tetherin HIV-1 interaction. *PLoS Pathogens* **7** e1002456

Lelek M, Di Nunzio F, Henriques R, Charneau P, Arhel N and Zimmer C 2012 Superresolution imaging of HIV in infected cells with FlAsH-PALM. *Proc. Natl. Acad. Sci.* **109** 8564–8569

Lin C-T and Ha T 2017 Probing single helicase dynamics on long nucleic acids through fluorescence-force measurement. *Methods Mol. Biol.* **1486** 295–316

Lin C-T, Tritschler F, Lee KS, Gu M, Rice CM and Ha T 2017 Single-molecule imaging reveals the translocation and DNA looping dynamics of hepatitis C virus NS3 helicase. *Protein Sci*. **26** 1391–1403

Lin C and Kim JL 1999 Structure-based mutagenesis study of hepatitis C virus NS3 helicase. *J. Virol.* **73** 8798–807

Liu S, Abbondanzieri EA, Rausch JW, Grice SFJL and Zhuang X 2008 Slide into action: dynamic shuttling of HIV reverse transcriptase on nucleic acid substrates. *Science* **322** 1092–1097

Los GV, Encell LP, McDougall MG, Hartzell DD, Karassina N, Zimprich C, Wood MG, Learish R, Ohana RF, Urh M, Simpson D, Mendez J, Zimmerman K, Otto P, Vidugiris G, Zhu J, Darzins A, Klaubert DH, Bulleit RF and Wood KV 2008 HaloTag: a novel protein labeling technology for cell imaging and protein analysis. *ACS Chem. Biol.* **3** 373–382

Lovatt D, Ruble BK, Lee J, Dueck H, Kim TK, Fisher S, Francis C, Spaethling JM Wolf JA, Grady MS, Ulyanova AV, Yeldell SB, Griepenburg JC, Buckley PT, Kim J, Sul JY, Dmochowski IJ and Eberwine J 2014 Transcriptome in vivo analysis (TIVA) of spatially defined single cells in live tissue. *Nat. Methods* **11** 190–196

Lubeck E and Cai L 2012 Single-cell systems biology by super-resolution imaging and combinatorial labeling. *Nat. Methods* **9** 743–748

Luo G, Wang M, Konigsberg WH and Xie XS 2007 Single-molecule and ensemble fluorescence assays for a functionally important conformational change in T7 DNA polymerase. *Proc. Natl. Acad. Sci. USA* **104** 12610–12615

Ma Y, Yates J, Liang Y, Lemon SM and Yi M 2008 NS3 helicase domains involved in infectious intracellular hepatitis C virus particle assembly. *J. Virol.* **82** 7624–7639

Maier G, Dietrich U, Panhans B, Schroder B, Rubsamen-Waigmann H, Cellai L, Hermann T and Heumann H 1999 Mixed reconstitution of mutated subunits of HIV-1 reverse transcriptase coexpressed in *Escherichia coli* - two tags tie it up. *European. J. Biochem.* **261** 10–18

Maier O, Sollars PJ, Pickard GE and Smith GA 2016 Visualizing herpesvirus procapsids in living cells. *J. Virol.* **90** 10182–10192

Maiti S, Haupts U and Webb WW 1997 Fluorescence correlation spectroscopy: Diagnostics for sparse molecules. *Proc. Natl. Acad. Sci.* **94** 11753–11757

Manley S, Gillette JM, Patterson GH, Shroff H, Hess HF, Betzig E and Lippincott-Schwartz J 2008 High-density mapping of single-molecule trajectories with photoactivated localization microscopy. *Nat. Methods* **5** 155–157

Mann DA, Mikaélian I, Zemmel RW, Green SM, Lowe AD, Kimura T, Singh M, Butler PJ, Gait MJ and Karn J 1994 A molecular rheostat. Co-operative rev binding to stem I of the rev-response element modulates human immunodeficiency virus type-1 late gene expression. *J. Mol. Biol.* **241** 193–207

Marko RA, Liu HW, Ablenas CJ, Ehteshami M, Götte M and Cosa G 2013 Binding kinetics and affinities of heterodimeric versus homodimeric HIV-1 reverse transcriptase on DNA-DNA substrates at the single-molecule level. *J. Phys. Chem. B* **117** 4560–4567

Marsh M and Helenius A 2006 Virus entry: Open sesame. *Cell* **124** 729–740

McKinney SA, Joo C and Ha T 2006 Analysis of single-molecule FRET trajectories using hidden Markov modeling. *Biophys. J.* **91** 1941–1951

Moerner WE and Fromm DP 2003 Methods of single-molecule fluorescence spectroscopy and microscopy. *Rev. Sci. Instrum.* **74** 3597–3619

Moffitt JR, Hao J, Wang G, Chen KH, Babcock HP and Zhuang X 2016 High-throughput single-cell gene-expression profiling with multiplexed error-robust fluorescence in situ hybridization. *Proc. Natl. Acad. Sci.* **113** 11046–11051

Müller B and Heilemann M 2013 Shedding new light on viruses: super-resolution microscopy for studying human immunodeficiency virus. *Trends Microbiol.* **21** 522–533

Munro JB, Gorman J, Ma X, Zhou Z, Arthos J, Burton DR, Koff WC, Courter JR, Smith AB, Kwong PD, Blanchard SC and Mothes W 2014 Conformational dynamics of single HIV-1 envelope trimers on the surface of native virions. *Science* **346** 759–763

Muranyi W, Malkusch S, Muller B, Heilemann M and Krusslich HG 2013 Super-resolution microscopy reveals specific recruitment of HIV-1 envelope proteins to viral assembly sites dependent on the envelope C-terminal tail. *PLoS Pathogens* **9** e1003198

Murray J, Savva CG, Shin B-S, Dever TE, Ramakrishnan V and Fernández IS 2016 Structural characterization of ribosome recruitment and translocation by type IV IRES. *eLife*. **5** e13567

Myong S, Bruno MM, Pyle AM and Ha T 2007 Spring-loaded mechanism of DNA unwinding by hepatitis C virus NS3 helicase. *Science* **317** 513–516

Myong S, Cui S, Cornish PV, Kirchhofer A, Gack MU, Jung JU, Hopfner K-P and Ha T 2009 Cytosolic viral sensor RIG-I is a 5'-

triphosphate-dependent translocase on double-stranded RNA. *Science* **323** 1070–1074

Nelles DA, Fang MY, O'Connell MR, Xu JL, Markmiller SJ, Doudna JA and Yeo GW 2016 Programmable RNA Tracking in Live Cells with CRISPR/Cas9. *Cell* **165** 488–496

Neuman KC and Nagy A 2008 Single-molecule force spectroscopy: Optical tweezers, magnetic tweezers and atomic force microscopy. *Nat. Methods* **5** 491–505

Ott M, Shai Y and Haran G 2013 Single-particle tracking reveals switching of the HIV fusion peptide between two diffusive modes in membranes. *J. Phys. Chem. B* **117** 13308–13321

Otterstrom J and van Oijen AM 2013 Visualization of membrane fusion, one particle at a time. *Biochemistry* **52** 1654–1668

Patel N, Wroblewski E, Leonov G, Phillips SEV, Tuma R, Twarock R and Stockley PG 2017 Rewriting nature's assembly manual for a ssRNA virus. *Proc. Natl. Acad. Sci.* **114** 12255–12260

Patterson G, Davidson M, Manley S and Lippincott-Schwartz J 2010 Superresolution imaging using single-molecule localization. *Annual. Rev. Phys. Chem.* **61** 345–367

Pelkmans L and Helenius A 2003 Insider information: what viruses tell us about endocytosis. *Curr. Opin. Cell. Biol.* **15** 414–22

Pelkmans L, Kartenbeck J and Helenius A 2001 Caveolar endocytosis of simian virus 40 reveals a new two-step vesicular-transport pathway to the ER. *Nat. Cell Biol.* **3** 473–483

Perlmutter JD and Hagan MF 2014 Mechanisms of virus assembly. *Annu. Rev. Phys. Chem.* **66** 217–239

Persson F, Lindén M, Unoson C and Elf J 2013 Extracting intracellular diffusive states and transition rates from single-molecule tracking data. *Nat. Methods* **10** 265–269

Pond SJK, Ridgeway WK, Robertson R, Wang J and Millar DP 2009 HIV-1 Rev protein assembles on viral RNA one molecule at a time. *Proc. Natl. Acad. Sci. USA* **106** 1404–1408

Prescher J, Baumgärtel V, Ivanchenko S, Torrano AA, Bräuchle C, Müller B and Lamb DC 2015 Super-resolution imaging of ESCRT-proteins at HIV-1 assembly sites. *PLoS Pathogens* **11** e1004677

Quan Y, Liang C, Inouye P and Wainberg MA 1998 Enhanced impairment of chain elongation by inhibitors of HIV reverse transcriptase in cell-free reactions yielding longer DNA products. *Nucleic Acids Res.* **26** 5692–5698

Ramanan V, Trehan K, Ong M-L, Luna JM, Hoffmann H-H, Espiritu C, Sheahan TP, Chandrasekar H, Schwartz RE, Christine KS, Rice CM, van Oudenaarden A and Bhatia SN 2016 Viral genome imaging of hepatitis C virus to probe heterogeneous viral infection and responses to antiviral therapies. *Virology* **494** 236–247

Ries J and Schwille P 2012 Fluorescence correlation spectroscopy. *BioEssays* **34** 361–368

Robb NC, te Velthuis AJW, Wieneke R, Tampé R, Cordes T, Fodor E and Kapanidis AN 2016 Single-molecule FRET reveals the pre-initiation and initiation conformations of influenza virus promoter RNA. *Nucleic Acids Res.* **44** gkw884

Robertson-Anderson RM, Wang J, Edgcomb SP, Carmel AB, Williamson JR and Millar DP 2011 Single-molecule studies reveal that DEAD box protein DDX1 promotes oligomerization of HIV-1 rev on the rev response element. *J. Mol. Biol.* **410** 959–971

Robertson JS 1979 5' and 3' terminal nucleotide sequences of the RNA genome segments of influenza virus. *Nucleic Acids Res.* **6** 3745–57

Routh A, Domitrovic T and Johnson JE 2012 Host RNAs, including transposons, are encapsidated by a eukaryotic single-stranded RNA virus. *Proc. Natl. Acad. Sci.* **109** 1907–1912

Roy R 2013 Next-generation optical microscopy. *Curr. Sci.* **105** 1524–1536

Roy R, Hohng S and Ha T 2008 A practical guide to single-molecule FRET. *Nat. Methods* **5** 507–516

Rust MJ, Lakadamyali M, Brandenburg B and Zhuang X 2011 Single-particle virus tracking. *Cold Spring Harb Protoc.* **2011** 1042–1055

Rust MJ, Lakadamyali M, Zhang F and Zhuang X 2004 Assembly of endocytic machinery around individual influenza viruses during viral entry. *Nat. Struct. Mol. Biol.* **11** 567–573

Sakin V, Hanne J, Dunder J, Anders-Össwein M, Laketa V, Nikić I, Kräusslich H-G, Lemke EA and Müller B 2017 A versatile tool for live-cell imaging and super-resolution nanoscopy studies of HIV-1 Env distribution and mobility. *Cell Chem. Biol.* **24** 635–645.e5

Sako Y, Minoghchi S and Yanagida T 2000 Single-molecule imaging of EGFR signalling on the surface of living cells. *Nat. Cell Biol.* **2** 168–172

Sarafianos SG, Das K, Tantillo C, Clark AD, Ding J, Whitcomb JM, Boyer PL, Hughes SH and Arnold E 2001 Crystal structure of HIV-1 reverse transcriptase in complex with a polypurine tract RNA:DNA. *EMBO J.* **20** 1449–1461

van Der Schaar HM, Rust MJ, Chen Van Der Ende-Metselaar H, Wilschut J, Zhuang X and Smit JM 2008 Dissecting the cell entry pathway of dengue virus by single-particle tracking in living cells. *PLoS Pathogens* **4** e1000244

van der Schaar HM, Rust MJ, Waarts B-L, van der Ende-Metselaar H, Kuhn RJ, Wilschut J, Zhuang X and Smit JM 2007 Characterization of the early events in dengue virus cell entry by biochemical assays and single-virus tracking. *J. Virol.* **81** 12019–12028

Schoggins JW, Dorner M, Feulner M, Imanaka N, Murphy MY, Ploss A and Rice CM 2012 Dengue reporter viruses reveal viral dynamics in interferon receptor-deficient mice and sensitivity to interferon effectors in vitro. *Proc. Natl. Acad. Sci. USA* **109** 14610–14615

Seisenberger G, Ried M U, Endress T, Büning H, Hallek M and Bräuchle C 2001 Real-time single molecule imaging of the infection pathway of an adeno-associated virus. *Science* **294** 1929–1932

Shah S, Lubeck E, Schwarzkopf M, He T-F, Greenbaum A, Sohn CH, Lignell A, Choi HMT, Gradinaru V, Pierce N A and Cai L 2016 Single-molecule RNA detection at depth by hybridization chain reaction and tissue hydrogel embedding and clearing. *Development* **143** 2862–2867

Shulla A and Randall G 2015 Spatiotemporal analysis of hepatitis C virus infection. *PLoS Pathogens* **11** 1–22

Sivaraman D, Biswas P, Cella LN, Yates MV and Chen W 2011 Detecting RNA viruses in living mammalian cells by fluorescence microscopy. *Trends Biotechnol.* **29** 307–313

Smith DE 2011 Single-molecule studies of viral DNA packaging. *Adv. Exp. Med. Biol.* **1** 134–141

Snijder B, Sacher R, Rämö P, Damm EM, Liberali P and Pelkmans L 2009 Population context determines cell-to-cell variability in endocytosis and virus infection. *Nature* **461** 520–523

Sood C, Francis AC, Desai TM and Melikyan GB 2017 An improved labeling strategy enables automated detection of

single-virus fusion and assessment of HIV-1 protease activity in single virions. *J. Biol. Chem.* **292** 20196–20207

Starnes M C, Gao W Y, Ting R Y and Cheng Y C 1988 Enzyme activity gel analysis of human immunodeficiency virus reverse transcriptase. *J. Biol. Chem* **263** 5132–5134

Stephens DJ and Allan VJ 2003 Light microscopy techniques for live cell imaging. *Science* **300** 82–86

Stockley PG, Twarock R, Bakker SE, Barker AM, Borodavka A, Dykeman E, Ford RJ, Pearson AR, Phillips SEV, Ranson NA and Tuma R 2013 Packaging signals in single-stranded RNA viruses: Nature's alternative to a purely electrostatic assembly mechanism. *J. Biol. Phys.* **39** 277–287

Sun E, He J and Zhuang X 2013 Live cell imaging of viral entry. *Curr. Opin. Virol.* **3** 34–43

Sun S, Rao VB and Rossmann MG 2010 Genome packaging in viruses. *Curr. Opin. Struct. Biol.* **20** 114–120

Tinoco I and Gonzalez RL 2011 Biological mechanisms, one molecule at a time. *Genes Dev.* **25** 1205–1231

Tokunaga M, Imamoto N and Sakata-Sogawa K 2008 Highly inclined thin illumination enables clear single-molecule imaging in cells. *Nat. Methods* **5** 159–161

Tomescu AI, Robb NC, Hengrung N, Fodor E and Kapanidis AN 2014 Single-molecule FRET reveals a corkscrew RNA structure for the polymerase-bound influenza virus promoter. *Proc. Natl. Acad. Sci.* **111** E3335–E3342

Vanover D, Smith DV, Blanchard EL, Alonas E, Kirschman JL, Lifland AW, Zurla C and Santangelo PJ 2017 RSV glycoprotein and genomic RNA dynamics reveal filament assembly prior to the plasma membrane. *Nat. Commun.* **8** 667

Venezia CF, Howard KJ, Ignatov ME, Holladay LA and Barkley MD 2006 Effects of Efavirenz binding on the subunit equilibria of HIV-1 reverse transcriptase. *Biochemistry* **45** 2779–2789

Walter NG, Huang C-Y, Manzo AJ and Sobhy MA 2008 Do-it-yourself guide: how to use the modern single-molecule toolkit. *Nat. Methods* **5** 475–489

Wang I-H, Suomalainen M, Andriasyan V, Kilcher S, Mercer J, Neef A, Luedtke NW and Greber UF 2013 Tracking viral genomes in host cells at single-molecule resolution. *Cell Host Microbe* **14** 468–480

Weiss S 1999 Fluorescence spectroscopy of single biomolecules. *Science* **283** 1676–83

Wessels L, Elting MW, Scimeca D and Weninger K 2007 Rapid membrane fusion of individual virus particles with supported lipid bilayers. *Biophys. J.* **93** 526–538

White JM and Whittaker GR 2016 Fusion of enveloped viruses in endosomes. *Traffic* **17** 593–614

Wichgers Schreur PJ and Kortekaas J 2016 Single-molecule FISH reveals non-selective packaging of rift valley fever virus genome segments. *PLoS Pathogens* **12** 1–21

Woolhouse MEJ and Gowtage-Sequeria S 2005 Host range and emerging and reemerging pathogens. *Emerging Infect. Diseases* **11** 1842–1847

Yang S-T, Kiessling V, Simmons JA, White JM and Tamm LK 2015 HIV gp41–mediated membrane fusion occurs at edges of cholesterol-rich lipid domains. *Nature. Chemi. Biol.* **11** 424–431

Yang S-T, Kreutzberger AJB, Lee J, Kiessling V and Tamm LK 2016 The role of cholesterol in membrane fusion. *Chem. Phys. Lipids* **199** 136–143

Zhang H, Ng M Y, Chen Y and Cooperman BS 2016 Kinetics of initiating polypeptide elongation in an IRES-dependent system. *eLife* **5** e13429

Zhou H-X, Rivas G and Minton AP 2008 Macromolecular crowding and confinement: biochemical, biophysical, and potential physiological consequences. *Annu. Rev. Biophys.* **37** 375–397

Zhou R, Schlierf M and Ha T 2010 Force-fluorescence spectroscopy at the single-molecule level. *Methods Enzymol.* **475** 405–426

Zlotnick A and Mukhopadhyay S 2011 Virus assembly, allostery and antivirals. *Trends Microbiol.* **19** 14–23